Comput. Aided Geom. Des. 109 (2024) 102276

Contents lists available at ScienceDirect

Computer Aided Geometric Design

journal homepage: www.elsevier.com/locate/cagd

Shape-preserving interpolation on surfaces via variable-degree splines

P.D. Kaklis [a,b], S. Stamatelopoulos [a,*], A.-A.I. Ginnis [c]

[a] Department of Naval Architecture, Ocean and Marine Engineering, University of Strathclyde, United Kingdom
[b] Foundation of Research & Technology - Hellas (FORTH), Institute of Applied and Computational Mathematics (IACM), Greece
[c] School of Naval Architecture and Marine Engineering, National Technical University of Athens, Greece

ARTICLE INFO

Keywords:
Shape-preserving interpolation on surfaces
Variable-degree splines
Geodesic curvature

ABSTRACT

This paper proposes two, geodesic-curvature based, criteria for shape-preserving interpolation on smooth surfaces, the first criterion being of non-local nature, while the second criterion is a local (weaker) version of the first one. These criteria are tested against a family of on-surface C^2 splines obtained by composing the parametric representation of the supporting surface with variable-degree (≥ 3) splines amended with the preimages of the shortest-path geodesic arcs connecting each pair of consecutive interpolation points. After securing that the interpolation problem is well posed, we proceed to investigate the asymptotic behaviour of the proposed on-surface splines as degrees increase. Firstly, it is shown that the local-convexity sub-criterion of the local criterion is satisfied. Second, moving to non-local asymptotics, we prove that, as degrees increase, the interpolant tends uniformly to the spline curve consisting of the shortest-path geodesic arcs. Then, focusing on isometrically parametrized developable surfaces, sufficient conditions are derived, which secure that all criteria of the first (strong) criterion for shape-preserving interpolation are met. Finally, it is proved that, for adequately large degrees, the aforementioned sufficient conditions are satisfied. This permits to build an algorithm that, after a finite number of iterations, provides a C^2 shape-preserving interpolant for a given data set on a developable surface.

1. Introduction

Shape Preservation (SP) in CAGD is any method of constructing a geometric entity, e.g., curve, surface, solid, that takes into account available shape information, e.g., monotonicity, convexity, moments of volume, the designer considers that have to be maintained throughout the geometric processing. For SP curves in the ambient space there exists an abundance of papers for the planar case, see, e.g., Augsdörfer et al. (2010), Costantini et al. (2010), Dyn et al. (1987), Dyn et al. (1992), Ferguson and Pruess (1991), Fletcher and McAllister (1986), Goodman and Unsworth (1988), Gregory (1986), Kaklis and Pandelis (1990), Kaklis and Sapidis (1995), Nyiri et al. (2011), Wever (1988), Yang (2006) for 2D SP-interpolation and Dierckx (1980), Dierckx (1996), Elfving and Anderson (1988), Elliott (1993), Juettler (1997), Kvasov (2000), Morandi et al. (2000), Pigounakis and Kaklis (1996), Schmidt and Scholz (1990), Wang and Xie (2022) for 2D SP-approximation. For spatial SP curves, pertinent literature is less extensive yet the reader can appeal to several works on 3D SP-interpolation, see, e.g., Costantini (2000), Costantini et al. (2001), Costantini and Manni

* Corresponding author.
E-mail address: stamatis@mit.edu (S. Stamatelopoulos).

https://doi.org/10.1016/j.cagd.2024.102276
Received 3 July 2023; Received in revised form 19 February 2024; Accepted 19 February 2024

Available online 28 February 2024

(2003), Goodman and Ong (1997), Kaklis and Karavelas (1997), Karavelas and Kaklis (2000), Lavery (2006) and Costantini and Pelosi (2001), Costantini and Pelosi (2004), Kong and Ong (2009) for 3D SP-approximation. These works exploit a broad spectrum of methods involving polynomial splines, rational splines, subdivision schemes and variational principles.

The problem of constructing SP interpolating/approximating (fitting) curves on surfaces, and more general on manifolds, is of practical interest in many domains, such as Geometric Modelling Azariadis and Aspragathos (2001), Patrikalakis and Bardis (1989), Computer Graphics Bennis et al. (1991) and Robotics Ma et al. (2020), Wu et al. (2016), Arvanitakis et al. (2013). In the latter domain of applications, which includes tool-machining on surfaces, inflection points are considered as the key CC (cutter-contact) points of the tool-axis vectors Ma et al. (2020). As for the analysis and control of robot motion on uneven terrains, the angular velocity of a robot is analogous to the geodesic curvature of its path Arvanitakis et al. (2013) and thus, extraneous inflection points of the geodesic curvature would result to abrupt and thus undesirable changes (jerks) Piazzi and Visioli (2000) in angular acceleration.

Nevertheless, SP interpolation/approximation on surfaces has not triggered so far research activity analogous to that of the corresponding baseline problem, namely interpolating on general Riemannian manifolds or special ones, such as the Lie group $SO(3)$ of rotations in $\mathbb{R}^3$; see, e.g., Camarinha et al. (2023), Gabriel and Kajiya (1985), Noakes et al. (1989). One should however refer to a line of works, see, e.g., Hofer and Pottmann (2004); Pottmann and Hofer (2005) and Bergmann and Gousenbourger (2018), which provide counterparts on surfaces of interpolating/fitting variational ambient splines. More specifically, the on-surface C^2 splines in tension, proposed in Hofer and Pottmann (2004); Pottmann and Hofer (2005), are SP-capable for, as tension parameters increase, they tend to the C^0-spline composed by the geodesic segments connecting the on-surface interpolation points. This spline ($\mathbf{\Gamma}$ in our terminology) provides the basis for introducing the notion of shape-preserving interpolation in our work (see Definition 1). Except from Dirichlet-integral minimizers which are only C^0, the C^2/C^4 on-surface cubic/quintic splines (Hofer and Pottmann, 2004; Pottmann and Hofer, 2005) are not SP in general for they prioritise, in analogy with their Euclidean counterparts, even spreading of curvature (lower-energy level) as opposed to curvature accumulation in the neighbourhood of the interpolation points, which occurs as tension increases. This is also the case for the work in Bergmann and Gousenbourger (2018), which derives a variational model to fit a C^1 composite on-surface Bézier curve against a set of points on a Riemannian manifold via minimising its mean squared (covariant) acceleration while remaining close to the interpolation points. The afore-mentioned counterparts are computed in discrete setting (pointwise), which renders the approach of Hofer and Pottmann (2004), Pottmann and Hofer (2005) and Bergmann and Gousenbourger (2018) incompatible with the continuous nature of the non-local criteria (i) and (ii) of Definition 1. One could, however, expect that it would be feasible to embed them in the local-convexity criterion (i) of Definition 2, which is essentially of discrete nature.

Another line of works with potential for SP interpolation/approximation on manifolds is that involving the non-linear generalisation of linear subdivision schemes for surfaces via, e.g., geodesic-means Wallner (2006), geodesic inductive averaging Dyn and Sharon (2017), Fréchet-means or exponential maps Wallner (2020), and non-stationary non-uniform schemes which enable smooth (C^2 limit curve) interpolation on manifolds Dyn et al. (2022). The discrete nature of these subdivision schemes imply that their embedding in the non-local-convexity criterion of our Definition 1 does not seem straightforward as it is likely the case with the local-convexity criterion of Definition 2. Furthermore, as pointed out in Dyn and Sharon (2017), those of the afore-mentioned subdivision schemes, that are based on the *proximity* concept, e.g., Wallnerand and Dyn (2005), Wallner (2006), are useful only for *"dense enough data", which is, in general, a condition that is hard to quantify and depends on the properties of the underline manifold (such as its curvature)*. On the contrary, the geodesic-inductive-averaging in Dyn and Sharon (2017) guarantees convergence from any initial manifold-valued sequence. Our approach is free from any *dense-enough-data* assumption, however, satisfying the *non-local-convexity criterion* (Definition 1) for non-developable surfaces depends on the parametrization of the underlying surface and its composition with a specific family of univariate splines (variable-degree splines), which is obviously not the case for subdivision schemes. One should, however, stress that the *local-convexity criterion* (Definition 2) is fulfilled by our method for general surfaces.

In this paper we start by proposing two criteria for shape-preserving interpolation on smooth surfaces, which are of geodesic-curvature character (Definition 1 & 2 in §2). Next, §3 introduces a family of on-surface splines via composing the surface parametric representation with the so-called variable-degree splines, amended with the preimages of the shortest-path geodesic arcs connecting each pair of consecutive interpolation points. After showing that the interpolation problem is well posed (Theorem 1), we proceed to study their local (§3.1) and global (§3.2) asymptotic behaviour as the degrees increase. In this connection, it is first proved that the local-convexity criterion of Definition 2 is satisfied (Theorem 2) for large degrees. Then, regarding their global asymptotic behaviour, Theorem 3 secures that, as degrees increase, the interpolant tends uniformly to the spline curve consisting of the shortest-path geodesic arcs. For the non-local-convexity criterion of Definition 1, however, one can provide different point sets on the same, non-developable, surface for which the proposed spline family succeeds (Example 2) or fails (Example 3) to satisfy the aforementioned criterion. In view of these experimental findings, §3.2.2 focuses on isometrically parametrized developable surfaces and derives sufficient conditions, securing that all criteria of Definition 1 are satisfied. Then, in §4 it is proved that, for adequately large degrees, the aforementioned sufficient conditions are satisfied (Theorem 7). This permits formulating Algorithm 1 with its performance illustrated in §5 against 4 data sets, 2 on a cone (see Examples 4, 5) and 2 on a cylinder (see Examples 6, 7). Finally, in §5.1, the impact of geodesic-length versus uniform parametrization associated to interpolation points is illustrated for 2 data sets.

2. Two criteria for shape-preserving interpolation on surfaces

Let be given a smooth parametric surface $\mathbf{S}(u,v)$, $(u,v) \in \Omega \subseteq \mathbb{R}^2$, and a set of points $\mathcal{I} = \{\mathbf{I}_i = \mathbf{S}(u_i,v_i),\ (u_i,v_i) \in \Omega, i = 0,1,...,n\}$ on it. We aim to set up a methodology for constructing smooth curves $\mathbf{c}(t)$, $t \in [t_0,t_n]$, that lie on $\mathbf{S}(u,v)$, interpolate the given points, $\mathbf{c}(t_i) = \mathbf{I}_i$, $i = 0,1,...,n$, on it, with t_i being user-specified parameters in $[t_0,t_n]$, and are *shape preserving*. Towards this aim we have

first to introduce and establish a notion of *shape-preserving interpolation on a surface*. For this purpose, we appeal to the shortest-path *geodesics* $\gamma_i(t)$, $t \in [t_i, t_{i+1}]$, that connect each consecutive pair of interpolation points with $\gamma_i(t_i) = \mathbf{I}_i$, $\gamma_i(t_{i+1}) = \mathbf{I}_{i+1}$, $i = 0, 1, ..., n-1$. This notion seems to provide a natural way for moving in a *continuous manner* from shape-preserving interpolation on the plane to that on a general (curved) surface. To start with, let us recall the definition of the *geodesic curvature* κ_g of a regular curve $\mathbf{c}(t)$ on $\mathbf{S}(u, v)$:

$$\kappa_g(t; \mathbf{c}) = \frac{(\dot{\mathbf{c}}(t), \ddot{\mathbf{c}}(t), \mathbf{n}(t))}{\|\dot{\mathbf{c}}(t)\|^3}, \tag{1}$$

where dot denotes differentiation with respect to the parameter t, $\mathbf{n}$ is the normal on $\mathbf{S}(u, v)$ at the point $\mathbf{c}(t) \in \mathbf{S}(u, v)$ and $(\mathbf{a}, \mathbf{b}, \mathbf{c})$ denotes the triple (mixed) scalar product of the vectors $\mathbf{a}$, $\mathbf{b}$ and $\mathbf{c}$. The above formula implies that κ_g measures the curvature of the projection of $\mathbf{c}(t)$ on the plane tangent to $\mathbf{S}(u, v)$ at the point under consideration. Curves for which $\kappa_g = 0$ are geodesic lines, e.g., linear segments on the plane, great-circle arcs on the sphere, etc.

In the planar case, the *shape-preserving interpolation criterion* in Kaklis and Sapidis (1995) is based on the sign sequence of the so-called *convexity indicators* $\mathrm{c}_{2D,i}$, $i = 1, ..., n-1$, at the vertices of the polygonal line $\mathbf{L}$ passing through the interpolation points $\mathbf{I}_i$, $i = 0, 1, ..., n$. More specifically, for any non-collinear triplet $\mathcal{I}_i = \{\mathbf{I}_m, m = i-1, i, i+1\}$, we have:

$$\mathrm{c}_{2D,i} = \frac{\mathbf{L}_{i-1} \times_{2D} \mathbf{L}_i}{\|\mathbf{L}_{i-1} \times_{2D} \mathbf{L}_i\|} = \pm 1, \quad \mathbf{L}_i = \mathbf{I}_{i+1} - \mathbf{I}_i, \quad i = 1, ..., n-1, \tag{2}$$

where $\mathbf{a} \times_{2D} \mathbf{b}$ denotes the projection of the typical vector product on the axis vertical to the plane defined by the vectors $\mathbf{a}$ and $\mathbf{b}$. In the case that the data set is closed ($\mathbf{I}_0 = \mathbf{I}_n$), $\mathrm{c}_{2D,i}$ can be defined for the two boundary points by setting $\mathbf{L}_{-1} = \mathbf{L}_n = \mathbf{I}_0 - \mathbf{I}_{n-1}$. Now, in view of (1), formula (2) can be alternatively written as:

$$\mathrm{c}_{2D,i} = \frac{(\mathbf{L}_{i-1}, \mathbf{L}_i, \mathbf{e}_3)}{\|\mathbf{L}_{i-1} \times_{2D} \mathbf{L}_i\|} = \pm 1, \tag{3}$$

where $\mathbf{e}_3$ is the unit normal on the plane defined by $\mathbf{L}_{i-1}$ and $\mathbf{L}_i$. The question then naturally arises if one can rationally extract (3) from (1) and exploit this path for introducing a notion of generalized convexity indicators c_i at the vertices of the curve $\mathbf{\Gamma}$, that lies on $\mathbf{S}(u, v)$ and consists of the shortest-path geodesic curves $\gamma_i(t)$, $t \in [t_i, t_{i+1}]$, $i = 0, 1, ..., n-1$, connecting consecutively the interpolation points $\mathbf{I}_i$, $i = 0, 1, ..., n$. For this purpose, assuming that $\mathbf{c}(t)$ is a regular and $C^2[t_0, t_n]$ curve, while the normal vector $\mathbf{n}(t)$ of $\mathbf{S}(u, v)$ is continuous in the neighbourhood of the interpolation points $\mathbf{I}_i$, $i = 0, ..., n$, we proceed to express the numerator in (1) at a knot t_i with the aid of a limit process around its full neighbourhood $U_i = [t_i - \Delta t, t_i + \Delta t]$. At first, we use left-hand side approximations for $\dot{\mathbf{c}}(t_i)$ and a first-order central divided-difference approximation of $\ddot{\mathbf{c}}(t)$. Then we get:

$$(\dot{\mathbf{c}}(t_i), \ddot{\mathbf{c}}(t_i), \mathbf{n}(t_i)) = \lim_{\Delta t \to 0} \left(\dot{\mathbf{c}}(t_i - \Delta t), \frac{\dot{\mathbf{c}}(t_i + \Delta t) - \dot{\mathbf{c}}(t_i - \Delta t)}{2\Delta t}, \mathbf{n}(t_i \pm \Delta t)\right) = \lim_{\Delta t \to 0} \frac{1}{2\Delta t} \left(\dot{\mathbf{c}}(t_i - \Delta t), \dot{\mathbf{c}}(t_i + \Delta t), \mathbf{n}(t_i \pm \Delta t)\right).$$

One can readily see that the above limit process remains invariant with respect to the chosen side, left or right, for approximating $\dot{\mathbf{c}}(t_i)$. Furthermore, if we assume that $\mathbf{S}(u, v)$ is smooth and locally orientable in the neighbourhood of the curve $\mathbf{\Gamma}$ we finally get:

$$(\dot{\mathbf{c}}(t_i), \ddot{\mathbf{c}}(t_i), \mathbf{n}(t_i)) = \lim_{\Delta t \to 0} \frac{1}{2\Delta t} \left(\dot{\mathbf{c}}(t_i - \Delta t), \dot{\mathbf{c}}(t_i + \Delta t), \mathbf{n}(t_i)\right). \tag{4}$$

On the basis of (4), we can say that, for sufficiently small Δt, the sign of the geodesic curvature $\kappa_g(t)$ of $\mathbf{c}(t)$ at a knot $t = t_i$ is governed by the sign of the quantity $(\dot{\mathbf{c}}(t_i - \Delta t), \dot{\mathbf{c}}(t_i + \Delta t), \mathbf{n}(t_i))$. Note that this quantity is appropriate for curves that are piecewise smooth, which is exactly the case for the curve $\mathbf{\Gamma}$.

Grounded on the above discussion, we introduce the sought-for notion of generalized convexity indicators c_i at the vertices $\mathbf{I}_i$ of the composite geodesic $\mathbf{\Gamma}$ on $\mathbf{S}(u, v)$ as follows:

$$\mathrm{c}_i = \frac{(\dot{\gamma}_{i-1}(t_i), \dot{\gamma}_i(t_i), \mathbf{n}(t_i))}{\|\dot{\gamma}_{i-1}(t_i) \times \dot{\gamma}_i(t_i)\|} = \pm 1, \tag{5}$$

under the assumption that the interpolation triplet $\mathcal{I}_i = \{\mathbf{I}_m, m = i-1, i, i+1\}$ does not belong on the same geodesic arc and $\gamma_{i-1}(t)$, $\gamma_i(t)$ have a regular parametrization. If $\mathbf{S}(u, v)$ is a planar surface then it is straightforward to show that (5) degenerates to (3).

Now, if the triplet $\mathcal{I}_i$ does belong on the same geodesic arc, then so will the geodesic arcs $\gamma_{i-1}(t)$ and $\gamma_i(t)$, referred to as *co-geodesics*, which implies that $\|\dot{\gamma}_{i-1}(t_i) \times \dot{\gamma}_i(t_i)\| = 0$ and

$$(\dot{\gamma}_{i-1}(t_i), \dot{\gamma}_i(t_i), \mathbf{n}(t_i)) = \left(\dot{\gamma}_{i-1}(t_i) \times \dot{\gamma}_i(t_i)\right) \cdot \mathbf{n}(t_i) = 0.$$

In that case, we extend (5) by setting $\mathrm{c}_i = 0$.

We are now ready to introduce the first criterion for shape-preserving interpolation surfaces:

Definition 1. Let be given a surface $\mathbf{S}(u, v)$, $(u, v) \in \Omega \subseteq \mathbb{R}^2$, and a set of points $\mathcal{I} = \{\mathbf{I}_i = \mathbf{S}(u_i, v_i), (u_i, v_i) \in \Omega, i = 0, 1, ..., n\}$ lying on it. Furthermore, let $\mathbf{\Gamma}$ be the composite curve consisting of the shortest-path geodesics $\gamma_i(t)$, $t \in [t_i, t_{i+1}]$, $i = 0, 1, ..., n-1$, connecting each pair of consecutive interpolation points, i.e., $\gamma_i(t_i) = \mathbf{I}_i$, $\gamma_i(t_{i+1}) = \mathbf{I}_{i+1}$, $i = 0, 1, ..., n-1$, where $\mathcal{T} = \{t_i, i = 0, 1, ..., n\}$ is a user-specified and strictly-increasing knot sequence. Under the assumption that $\mathbf{S}(u, v)$ is smooth (at least G^1-continuous) and locally orientable in

the neighbourhood of the curve $\mathbf{\Gamma}$, a smooth (at least twice-differentiable) regular curve $\mathbf{c}(t)$ lying on $\mathbf{S}(u,v)$ and interpolating $\mathcal{I}$, i.e., $\mathbf{c}(t_i)=\mathbf{I}_i$, $i=0,1,...,n$, will be called *shape-preserving interpolant* provided that:

(i) Non-local-convexity criterion: if $\mathrm{c}_m\mathrm{c}_{m+1}>0$ then

$$\kappa_g(t;\mathbf{c})\mathrm{c}_n>0,\quad t\in[t_m,t_{m+1}],n=m \text{ or } m+1. \tag{6}$$

(ii) Minimum-variation criterion: if $\mathrm{c}_m\mathrm{c}_{m+1}<0$ then

$$\kappa_g(t;\mathbf{c})\mathrm{c}_m\geq 0,\ t\in[t_m,\xi_m],\quad \kappa_g(t;\mathbf{c})\mathrm{c}_{m+1}\geq 0,\ t\in[\xi_m,t_{m+1}], \tag{7}$$

for some $\xi_m\in(t_m,t_{m+1})$.

(iii) Local-co-geodesity criterion: if $\mathrm{c}_m=0$ and $\dot\gamma_{m-1}(t_m)\cdot\dot\gamma_m(t_m)>0$, then there exists a neighbourhood $\eta_m\subset(t_{m-1},t_{m+1})$ of t_m, such that

$$\|\dot{\mathbf{c}}(t)\times\dot\gamma_l(t_m)\|\leq\delta \tag{8}$$

where δ is a user-specified small positive number in $(0,1]$ and $l=m-1,\ m$.

Part (i) of the above Definition 1 is the analogue of the criteria introduced in Kaklis and Sapidis (1995) (Def. 3.1.(i)) and Kaklis and Karavelas (1997) (Def. 2.1.(i)) for planar/spatial shape-preserving interpolation, respectively. In this work, the sign of the geodesic curvature is used in place of the sign of the curvature for the planar and the variation of the binormal for the 3D case. Via part (ii) of Definition 1, the proposed criterion aims to minimise the variation of the geodesic curvature when consecutive generalised convexity indicators are of opposite sign. Finally, Part (iii) of Definition 1 resembles the criteria in Kaklis and Sapidis (1995) (Def. 3.1.(ii)) and Kaklis and Karavelas (1997) (Def. 2.1.(iv)) by enforcing the interpolant to be sufficiently close to the co-geodesic arcs in a user-specified neighbourhood of the intermediate interpolation point. Note that the case $\mathrm{c}_m=0$ with $\dot\gamma_{m-1}(t_m)\cdot\dot\gamma_m(t_m)<0$, should not be associated with co-geodesic behaviour, since such triplets are more likely to imply cusp-like behaviour.

We end this section by stating the second criterion for shape-preserving interpolation surfaces, which is a weaker (local) version of the previous criterion:

Definition 2. Under the hypotheses of Definition 1, the curve $\mathbf{c}(t)$ will be called *locally shape-preserving interpolant* provided that

(i) Local-convexity criterion: If $\mathrm{c}_\ell\neq 0$, then there exists a neighbourhood $\theta_\ell\subset(t_{\ell-1},t_{\ell+1})$ of t_ℓ, such that

$$\kappa_g(t;\mathbf{c})\mathrm{c}_\ell>0,\quad t\in\theta_\ell. \tag{9}$$

(ii) Local-co-geodesity criterion: As in (iii) in Definition 1.

3. A geodesic-based family of C^2-continuous interpolatory curves on surfaces

The members $\mathbf{c}(t)$ of this family are defined by composing $\mathbf{S}(u,v)$ with a family of planar curves, $\mathbf{q}(t)$, which combine the shape-preserving interpolation properties of the so-called *polynomial splines of non-uniform degree*, Kaklis and Sapidis (1995), Kaklis and Karavelas (1997), with the preimage

$$\mathbf{g}_i(t)=\mathbf{S}^{-1}(\gamma_i(t)) \tag{10}$$

of the geodesic arcs $\gamma_i(t)$, referred to in Definition 1. More accurately,

$$\mathbf{c}(t)=(\mathbf{S}\circ\mathbf{q})(t), \tag{11}$$

where

$$\mathbf{q}(t)=\mathbf{g}_i(t)+h_i^2(\ddot{\mathbf{q}}_i-\ddot{\mathbf{g}}_i(t_i))F_i(1-\tau)+h_i^2(\ddot{\mathbf{q}}_{i+1}-\ddot{\mathbf{g}}_i(t_{i+1}))F_i(\tau),\ t\in[t_i,t_{i+1}],\ \ddot{\mathbf{q}}_i:=d^2\mathbf{q}(t_i)/dt^2, \tag{12a}$$

$$F_i(\tau)=\frac{\tau^{k_i}-\tau}{k_i(k_i-1)},\quad 3\leq k_i\in\mathbb{N},\quad \tau=\frac{t-t_i}{h_i}\in[0,1],\ h_i=t_{i+1}-t_i,\ i=0,...,n-1, \tag{12b}$$

with the dot superscript denoting differentiation with respect to the global parameter t. The above formula defines planar splines in the (u,v)-plane that interpolate the preimages $\mathbf{P}_i=\mathbf{S}^{-1}(\mathbf{I}_i)$ of the interpolation points $\mathbf{I}_i$ on the surface $\mathbf{S}$ and can inherit, as it will be shown in the forthcoming sections, shape-information from the preimage curves $\mathbf{g}_i(t)$, $i=0,1,...,n-1$. Note that, per parametric interval $[t_i,t_{i+1}]$, $\mathbf{q}(t)$ contains a polynomial part of non-uniform degree, k_i, $i=0,1,...,n-1$; see the 2^{nd} and 3^{rd} term in the right hand side of (12a). Finally, the *on-surface* curves $\mathbf{c}(t)$ will be henceforth considered to be C^2-continuously differentiable on $[t_i,t_{i+1}]$, as a result of the below assumptions:

Assumption 1. $\mathbf{S}(u,v)$ is at least C^2-continuously differentiable on $\Omega\ni(u,v)$ and locally bijective in the neighbourhood of the curve Γ.

Assumption 2. The geodesic components $\gamma_i(t)$ of the composite curve $\mathbf{\Gamma}$ are C^2-continuously differentiable on $[t_i, t_{i+1}] \ni t$.

Now, regarding the interpolation properties of $\mathbf{q}(t)$ we readily have:

$$\mathbf{q}(t_i) = \mathbf{g}_i(t_i) + h_i^2(\ddot{\mathbf{q}}_i - \ddot{\mathbf{g}}_i(t_i))F_i(1) + h_i^2(\ddot{\mathbf{q}}_{i+1} - \ddot{\mathbf{g}}_i(t_{i+1}))F_i(0) = \mathbf{g}_i(t_i) = \mathbf{P}_i,$$

as a result of the fact that $F_i(0) = F_i(1) = 0$. Furthermore, since $F''(0) = 0$ and $F''(1) = 1$, with the prime superscript denoting differentiation with respect to the local variable τ, we readily confirm that

$$\lim_{\Delta t \to 0} \ddot{\mathbf{q}}(t_i + \Delta t) \equiv \ddot{\mathbf{q}}(t_i^+) = \ddot{\mathbf{q}}_i, \quad \lim_{\Delta t \to 0} \ddot{\mathbf{q}}(t_{i+1} - \Delta t) \equiv \ddot{\mathbf{q}}(t_{i+1}^-) = \ddot{\mathbf{q}}_{i+1}. \tag{13}$$

Then, aiming to secure that $\mathbf{q}(t) \in C^2(I)$, $I = [t_0, t_n]$, it only suffices to ensure that $\dot{\mathbf{q}}(t_i^-) = \dot{\mathbf{q}}(t_i^+)$ for all interior nodes $t_i, i = 1, ..., n-1$. Formulae (12) then give:

$$\dot{\mathbf{q}}(t) = \dot{\mathbf{g}}_i(t) - h_i(\ddot{\mathbf{q}}_i - \ddot{\mathbf{g}}_i(t_i))F_i'(1-\tau) + h_i(\ddot{\mathbf{q}}_{i+1} - \ddot{\mathbf{g}}_i(t_{i+1}))F_i'(\tau), \quad \tau = \frac{t - t_i}{h_i}, \; t \in [t_i, t_{i+1}], \tag{14a}$$

for the subinterval on the right of an internal node t_i and analogously

$$\dot{\mathbf{q}}(t) = \dot{\mathbf{g}}_{i-1}(t) - h_{i-1}(\ddot{\mathbf{q}}_{i-1} - \ddot{\mathbf{g}}_{i-1}(t_{i-1}))F_{i-1}'(1-\tau) + h_{i-1}(\ddot{\mathbf{q}}_i - \ddot{\mathbf{g}}_{i-1}(t_i))F_{i-1}'(\tau), \quad \tau = \frac{t - t_{i-1}}{h_{i-1}}, \; t \in [t_{i-1}, t_i], \tag{14b}$$

for the subinterval on the left of an internal node t_i. Then, setting $t = t_i$ ($\tau = 0$) in (14a) we get:

$$\dot{\mathbf{q}}(t_i^+) = \dot{\mathbf{g}}_i(t_i) - h_i(\ddot{\mathbf{q}}_i - \ddot{\mathbf{g}}_i(t_i))F_i'(1) + h_i(\ddot{\mathbf{q}}_{i+1} - \ddot{\mathbf{g}}_i(t_{i+1}))F_i'(0), \tag{15a}$$

while for $t = t_i$ ($\tau = 1$), (14b) gives

$$\dot{\mathbf{q}}(t_i^-) = \dot{\mathbf{g}}_{i-1}(t_i) - h_{i-1}(\ddot{\mathbf{q}}_{i-1} - \ddot{\mathbf{g}}_{i-1}(t_{i-1}))F_{i-1}'(0) + h_{i-1}(\ddot{\mathbf{q}}_i - \ddot{\mathbf{g}}_{i-1}(t_i))F_{i-1}'(1). \tag{15b}$$

Using formulae (15) the continuity constraints $\dot{\mathbf{q}}(t_i^-) = \dot{\mathbf{q}}(t_i^+)$, $i = 1, ..., n-1$, can be written as:

$$\begin{aligned} &- h_{i-1}\ddot{\mathbf{q}}_{i-1}F_{i-1}'(0) + h_{i-1}\ddot{\mathbf{q}}_i F_{i-1}'(1) + h_i\ddot{\mathbf{q}}_i F_i'(1) - h_i\ddot{\mathbf{q}}_{i+1}F_i'(0) = \\ &\quad \dot{\mathbf{g}}_i(t_i) - \dot{\mathbf{g}}_{i-1}(t_i) - h_{i-1}\ddot{\mathbf{g}}_{i-1}(t_{i-1})F_{i-1}'(0) + h_{i-1}\ddot{\mathbf{g}}_{i-1}(t_i)F_{i-1}'(1) + h_i\ddot{\mathbf{g}}_i(t_i)F_i'(1) - h_i\ddot{\mathbf{g}}_i(t_{i+1})F_i'(0), \quad i = 1, ..., n-1, \end{aligned}$$

which, in view of the fact that

$$F_i'(0) = -\frac{1}{k_i(k_i - 1)}, \quad F_i'(1) = \frac{1}{k_i},$$

takes the following final form:

$$e_{i-1}\ddot{\mathbf{q}}_{i-1} + (d_i + d_{i-1})\ddot{\mathbf{q}}_i + e_i\ddot{\mathbf{q}}_{i+1} = \dot{\mathbf{g}}_i(t_i) - \dot{\mathbf{g}}_{i-1}(t_i) + e_{i-1}\ddot{\mathbf{g}}_{i-1}(t_{i-1}) + d_{i-1}\ddot{\mathbf{g}}_{i-1}(t_i) + d_i\ddot{\mathbf{g}}_i(t_i) + e_i\ddot{\mathbf{g}}_i(t_{i+1}), \quad i = 1, ..., n-1, \tag{16a}$$

where

$$e_i = h_i/k_i(k_i - 1), \quad d_i = h_i/k_i. \tag{16b}$$

In direct analogy with Kaklis and Sapidis (1995), equations (16) endowed with appropriate boundary conditions $\mathcal{B}$ at $t = t_0$ and $t = t_n$, lead to a linear system of $n+1$ equations for $n+1$ unknowns, namely the second-order nodal derivatives $\ddot{\mathbf{q}}_i$, $i = 0, 1, ..., n$. This symmetric system is uniquely solvable for the associated matrix is strictly diagonally dominant as a result of the fact that:

$$d_i > e_i, \quad k_i \geq 3, \; i = 0, ..., n-1.$$

In summary we can state:

Theorem 1. *Let be given a surface* $\mathbf{S}(u, v)$ $(u, v) \in \Omega \subseteq \mathbb{R}^2$, *along with a set* $\mathcal{I} = \{\mathbf{I}_0, ..., \mathbf{I}_n\}$ *of points on it, a user-specified knot sequence* $\mathcal{T} = \{t_i : t_i < t_{i+1}, i = 0, 1, ..., n-1\}$ *and a set* $\mathcal{K} = \{k_0, ..., k_{n-1}\}$, $3 \leq k_i \in \mathbb{N}$, $i = 0, ..., n-1$. *Furthermore, let* $\mathbf{S}(u, v)$ *be locally orientable in the neighbourhood of the points of* $\mathcal{I}$ *and obey Assumption 1 while* $\mathbf{\Gamma}$, *the composite curve consisting of the shortest-path geodesics* $\gamma_i(t)$, $t \in [t_i, t_{i+1}]$, $i = 0, 1, ..., n-1$, *connecting consecutively the points of* $\mathcal{I}$, *obeys Assumption 2. Then, under appropriate boundary conditions* $\mathcal{B}$, *there exists a unique curve* $\mathbf{c}(t) \in C^2([t_0, t_n])$ *represented as in (11), which lies on* $\mathbf{S}(u, v)$ *and interpolates* $\mathcal{I}$ *in conformity with the knot sequence* $\mathcal{T}$.

3.1. Local asymptotic behaviour

Let us consider that the degrees, k_{i-1} and k_i, in two neighbouring parametric intervals, $[t_{i-1}, t_i]$ and $[t_i, t_{i+1}]$, increase so that

$$\lim_{k_{i-1},k_i\to\infty} \frac{k_{i-1}}{k_i} = \kappa_i, \tag{17}$$

where κ_i are prefixed non-zero positive constants. Appealing to an asymptotic result that holds true in the case of planar curves of non-uniform degree (see Lemma 3.1 in Kaklis and Sapidis, 1995) and taking into account that, as $k_i, k_{i-1} \to \infty$, the right-hand side in (16a) tends to $\dot{\mathbf{g}}_i(t_i) - \dot{\mathbf{g}}_{i-1}(t_i)$, (16a) can take the form:

$$(d_{i-1} + d_i)\ddot{\mathbf{q}}_i = \mathbf{R}_i \quad \text{with} \lim_{k_{i-1},k_i\to\infty} \mathbf{R}_i = \dot{\mathbf{g}}_i(t_i) - \dot{\mathbf{g}}_{i-1}(t_i). \tag{18}$$

We shall now exploit (18) for extracting an analogous asymptotic estimate for the one-sided tangent vectors $\dot{\mathbf{q}}(t_i\pm)$, defined by formulae (15). Since (16a) secures the continuity of $\dot{\mathbf{q}}(t)$ in the neighbourhood of the nodes t_i, it suffices to perform the asymptotics for $\dot{\mathbf{q}}(t_i^+)$. To proceed, we rewrite (15a) in the following way:

$$\dot{\mathbf{q}}(t_i^+) = \dot{\mathbf{g}}_i(t_i) - h_i\mathbf{R}_i \frac{1}{d_{i-1}+d_i}\cdot\frac{1}{k_i} + h_i\ddot{\mathbf{g}}_i(t_i)\frac{1}{k_i} - h_i\mathbf{R}_{i+1}\frac{1}{d_i+d_{i+1}}\cdot\frac{1}{k_i(k_i-1)} + h_i\ddot{\mathbf{g}}_i(t_{i+1})\frac{1}{k_i(k_i-1)}. \tag{19}$$

Obviously, the 3^{rd} and 5^{th} terms in the right-hand side of the above formula tend to zero as $k_j \to \infty$, $j = i-1, i$. For the 4^{th} term, appealing again to Lemma 3.1 (Kaklis and Sapidis, 1995), we can state:

$$\|\mathbf{R}_{i+1}\| \le M, \tag{20a}$$

where M is a constant depending on the point set $\mathcal{I}$, the parametrization $\mathcal{T}$, and the boundary conditions $\mathcal{B}$. As for the multiplier f_i of $\mathbf{R}_{i+1}$ in the right-hand side of (19) we easily get the following bound:

$$\|f_i\| = h_i\frac{1}{d_i+d_{i+1}}\cdot\frac{1}{k_i(k_i-1)} \le h_i\frac{1}{d_i}\cdot\frac{1}{k_i(k_i-1)} = \frac{1}{k_i-1}. \tag{20b}$$

On the basis of (20) we conclude that the 4^{th} term in the right-hand side of (19) tends also to zero as $k_j \to \infty$, $j = i-1, i$. Collecting the results obtained so far, we have

$$\lim_{k_i,k_{i-1}\to\infty} \dot{\mathbf{q}}(t_i^+) = \dot{\mathbf{g}}_i(t_i) - \lim_{k_i,k_{i-1}\to\infty}\left[h_i\mathbf{R}_i\frac{1}{d_{i-1}+d_i}\cdot\frac{1}{k_i}\right] = \dot{\mathbf{g}}_i(t_i) - (\dot{\mathbf{g}}_i(t_i) - \dot{\mathbf{g}}_{i-1}(t_i))\cdot\frac{1}{1+\frac{h_{i-1}}{h_i}\cdot\frac{1}{\kappa_i}}.$$

In more compact form, the above asymptotic limit can be written as

$$\lim_{k_i,k_{i-1}\to\infty} \dot{\mathbf{q}}(t_i^+) = (1-\lambda_i)\dot{\mathbf{g}}_i(t_i) + \lambda_i\dot{\mathbf{g}}_{i-1}(t_i), \tag{21a}$$

where

$$\lambda_i = \frac{1}{1+\frac{h_{i-1}}{h_i}\cdot\frac{1}{\kappa_i}} < 1. \tag{21b}$$

Summarising, under the assumption that the degrees k_{i-1} and k_i increase in alignment with the bound (17), the limit of $\dot{\mathbf{q}}(t_i^+)$ is expressed as a convex combination of the first-order derivatives at $t = t_i$ of the preimages $\mathbf{g}_{i-1}(t)$, $\mathbf{g}_i(t)$ of the neighbouring geodesics $\gamma_{i-1}(t)$ and $\gamma_i(t)$, respectively. Formulae (21) hold true for $\dot{\mathbf{q}}(t_i^-)$ as well, as a result of the C^1-continuity secured in the neighbourhood of the nodes t_i.

We shall now exploit the asymptotic relations (18) and (21) for investigating the corresponding asymptotic behaviour of the geodesic curvature of the curve $\mathbf{c}(t)$ in the neighbourhood of the interpolation point $\mathbf{I}_i = \mathbf{c}(t_i)$. For this purpose we first set $\mathbf{q}(t) = (u(t), v(t))^T$ and then, appealing to (11), we get the following standard formulae for the first two derivatives of $\mathbf{c}(t)$:

$$\dot{\mathbf{c}}(t) = \mathbf{S}_u\dot{u} + \mathbf{S}_v\dot{v}, \tag{22}$$

$$\ddot{\mathbf{c}}(t) = \mathbf{S}_u\ddot{u} + \mathbf{S}_v\ddot{v} + \mathbf{r}(u,v), \text{ where } \quad \mathbf{r}(u,v) = \mathbf{S}_{uu}(\dot{u})^2 + 2\mathbf{S}_{uv}\dot{u}\dot{v} + \mathbf{S}_{vv}(\dot{v})^2, \tag{23}$$

and, in more compact form:

$$(\dot{\mathbf{c}}(t), \ddot{\mathbf{c}}(t), \mathbf{n}) = (\dot{u}\ddot{v} - \dot{v}\ddot{u})(\mathbf{S}_u, \mathbf{S}_v, \mathbf{n}) + (\mathbf{S}_u\dot{u} + \mathbf{S}_v\dot{v}, \mathbf{r}, \mathbf{n}) := \dot{\mathbf{q}}(t) \times_{2D} \ddot{\mathbf{q}}(t)(\mathbf{S}_u, \mathbf{S}_v, \mathbf{n}) + (\mathbf{S}_u\dot{u} + \mathbf{S}_v\dot{v}, \mathbf{r}, \mathbf{n}). \tag{24}$$

Now, using the expression of $\mathbf{r}(u,v)$, given in (23), for rewriting the second term in the right-hand side of (24), we obtain:

$$\begin{aligned}(\mathbf{S}_u\dot{u} + \mathbf{S}_v\dot{v}, \mathbf{r}, \mathbf{n}) = (\mathbf{S}_u\dot{u} + \mathbf{S}_v\dot{v}, \mathbf{S}_{uu}(\dot{u})^2 + 2\mathbf{S}_{uv}\dot{u}\dot{v} + \mathbf{S}_{vv}(\dot{v})^2, \mathbf{n}) = (\dot{u})^3(\mathbf{S}_u, \mathbf{S}_{uu}, \mathbf{n}) + 2(\dot{u})^2\dot{v}(\mathbf{S}_u, \mathbf{S}_{uv}, \mathbf{n}) + \dot{u}(\dot{v})^2(\mathbf{S}_u, \mathbf{S}_{vv}, \mathbf{n}) + \\ + (\dot{u})^2\dot{v}(\mathbf{S}_v, \mathbf{S}_{uu}, \mathbf{n}) + 2\dot{u}(\dot{v})^2(\mathbf{S}_v, \mathbf{S}_{uv}, \mathbf{n}) + (\dot{v})^3(\mathbf{S}_v, \mathbf{S}_{vv}, \mathbf{n}).\end{aligned} \tag{25}$$

Let us now multiply both sides of (24) by $(d_{i-1}+d_i)$ and study its behaviour as $k_{i-1},k_i\to\infty$ at $t=t_i$, equivalently at the surface point $\mathbf{I}_i=\mathbf{S}(u(t_i),v(t_i))$. We then can write:

$$\lim_{k_{i-1},k_i\to\infty}((d_{i-1}+d_i))(\dot{\mathbf{c}}(t_i),\ddot{\mathbf{c}}(t_i),\mathbf{n}(\mathbf{I_i}))=\lim_{k_{i-1},k_i\to\infty}\left[\dot{\mathbf{q}}(t_i)\times_{2D}((d_{i-1}+d_i)\ddot{\mathbf{q}}(t_i))\right](\mathbf{S}_u(\mathbf{I}_i),\mathbf{S}_v(\mathbf{I}_i),\mathbf{n}(\mathbf{I}_i))+$$
$$\lim_{k_{i-1},k_i\to\infty}\left[(d_{i-1}+d_i)(\mathbf{S}_u(\mathbf{I}_i)\dot{u}(t_i)+\mathbf{S}_v(\mathbf{I}_i)\dot{v}(t_i),\mathbf{r}(\mathbf{I}_i),\mathbf{n}(\mathbf{I}_i)\right]. \tag{26}$$

Then, combining (25) with (21) and (18), we can get the following asymptotic estimate for the right-hand side of (26):

$$\lim_{k_{i-1},k_i\to\infty}((d_{i-1}+d_i))(\dot{\mathbf{c}}(t_i),\ddot{\mathbf{c}}(t_i),\mathbf{n}(\mathbf{I_i}))=[(1-\lambda_i)\dot{\mathbf{g}}_i(t_i)+\lambda_i\dot{\mathbf{g}}_{i-1}(t_i)]\times_{2D}[\dot{\mathbf{g}}_i(t_i)-\dot{\mathbf{g}}_{i-1}(t_i)](\mathbf{S}_u(\mathbf{I}_i),\mathbf{S}_v(\mathbf{I}_i),\mathbf{n}(\mathbf{I}_i))+O(k_{i-1}^{-1},k_i^{-1})=$$
$$=[\dot{\mathbf{g}}_{i-1}(t_i)\times_{2D}\dot{\mathbf{g}}_i(t_i)](\mathbf{S}_u(\mathbf{I}_i),\mathbf{S}_v(\mathbf{I}_i),\mathbf{n}(\mathbf{I}_i))+O(k_{i-1}^{-1},k_i^{-1}). \tag{27}$$

On the basis of the orientability assumption in Theorem 1, it is legitimate to say that a consistent concept of clockwise rotation can be defined on the surface in a continuous manner so that the scalar triple product retains constant sign, say positive, along $\mathbf{\Gamma}$, i.e.,

$$(\mathbf{S}_u(\mathbf{I}_i),\mathbf{S}_v(\mathbf{I}_i),\mathbf{n}(\mathbf{I}_i))=\|\mathbf{S}_u(\mathbf{I}_i)\times\mathbf{S}_v(\mathbf{I}_i)\|. \tag{28}$$

Consequently, on the basis of (27) and (28), we are led to

Lemma 1. *If k_{i-1},k_i increase in compatibility with (17), then the geodesic curvature of $\mathbf{c}(t)$ at $t=t_i$ and the quantity $\dot{\mathbf{g}}_{i-1}(t_i)\times_{2D}\dot{\mathbf{g}}_i(t_i)$ will share the same sign for sufficiently large degrees.*

The question then naturally arises about the liaison between the quantity $\dot{\mathbf{g}}_{i-1}(t_i)\times_{2D}\dot{\mathbf{g}}_i(t_i)$ and the generalised convexity indicator c_i defined by (5) and used in part (i) of the shape preserving interpolation criteria for data on surfaces introduced in Definitions 1 and 2. Since $\gamma_j(t)=\mathbf{S}(\mathbf{g}_j(t))$, $\mathbf{g}_j=(g_j^u(t),g_j^v(t))^T$, and recalling the standard relation (see also (22))

$$\dot{\gamma}_j(t)=\mathbf{S}_u\dot{g}_j^u(t)+\mathbf{S}_v\dot{g}_j^v(t),$$

we have:

$$\dot{\gamma}_{i-1}(t_i)\times\dot{\gamma}_i(t_i)=(\mathbf{S}_u(\mathbf{I}_i)\dot{g}_{i-1}^u(t_i)+\mathbf{S}_v(\mathbf{I}_i)\dot{g}_{i-1}^v(t_i))\times(\mathbf{S}_u(\mathbf{I}_i)\dot{g}_i^u(t_i)+\mathbf{S}_v(\mathbf{I}_i)\dot{g}_i^v(t_i))=[\dot{\mathbf{g}}_{i-1}(t_i)\times_{2D}\dot{\mathbf{g}}_i(t_i)]\mathbf{S}_u(\mathbf{I}_i)\times\mathbf{S}_v(\mathbf{I}_i)\Rightarrow \tag{29}$$

$$(\dot{\gamma}_{i-1}(t_i),\dot{\gamma}_i(t_i),\mathbf{n}(t_i))=[\dot{\mathbf{g}}_{i-1}(t_i)\times_{2D}\dot{\mathbf{g}}_i(t_i)](\mathbf{S}_u(\mathbf{I}_i),\mathbf{S}_v(\mathbf{I}_i),\mathbf{n}(t_i)), \tag{30}$$

which, in view of (28), gives

$$\mathrm{sign}(\dot{\gamma}_{i-1}(t_i),\dot{\gamma}_i(t_i),\mathbf{n}(t_i))=\mathrm{sign}[\dot{\mathbf{g}}_{i-1}(t_i)\times_{2D}\dot{\mathbf{g}}_i(t_i)]. \tag{31}$$

Combining (31) with (5), Lemma 1 and taking into account that the geodesic curvature $\kappa_g(t;\mathbf{c})$ is continuous, we can state:

Theorem 2. *If k_{i-1},k_i increase in compatibility with (17), then the geodesic curvature of $\mathbf{c}(t)$ at $t=t_i$ and the generalised convexity indicator c_i will share the same sign for sufficiently large degrees and thus the local-convexity criterion (i) in Definition 2 is satisfied.*

Example 1. A demonstration of Theorem 2 is documented in Table 1 and Figs. 1, 2, 3 and 4. For this example as well as Examples 2 and 3, the shortest-path geodesic preimages $\mathbf{g}_i$, $i=0,\ldots,n-1$, have been calculated by numerically solving their defining equations, also called *geodesic-equations* (35), in MAPLE®. It is easily verifiable that the geodesics produced by MAPLE® are indeed the shorter segment of the great-arcs connecting consecutive points thus securing the shortest-length property. Next, the on-surface renders for all examples have been generated in Rhino®. Fig. 1 shows two on-sphere members of the curve family (11). Specifically, the interval degrees of the spline in Fig. 1a are uniformly equal to 3, while for that of Fig. 1b they have all been increased to 6. As one can readily notice from Fig. 3, where the geodesic curvature of the two splines is plotted, the initial spline (all degrees equal to 3) fails the local-convexity criterion in Definition 2 at $t=0,2,4,6$. However, as predicted by Theorem 2, when increasing the interval degrees (all degrees equal to 6) the sign of the geodesic curvature at the interpolation points matches that of the respective convexity indicator. Furthermore, it also happens that the minimum-variation criterion in Definition 1 is satisfied.

3.2. Non-local asymptotic behaviour

3.2.1. Preamble

In the ensuing subsection (§3.2.2) we investigate and prove that the family of splines $\mathbf{c}(t)$, $t\in[t_0,t_n]$, introduced in §3 (see equation (11)), is capable to satisfy all criteria of Definition 1 for shape-preserving interpolation on developable surfaces. For general surfaces it is straightforward to prove (see Theorem 3 below) that, as degrees increase, $\mathbf{c}(t)$ tends uniformly to the curve $\mathbf{\Gamma}$, that lies on $\mathbf{S}(u,v)$ and consists of the shortest-path geodesic curves $\gamma_i(t)$, $t\in[t_i,t_{i+1}]$, $i=0,1,\ldots,n-1$, connecting consecutively the interpolation points $\mathbf{I}_i$, $i=0,1,\ldots,n$.

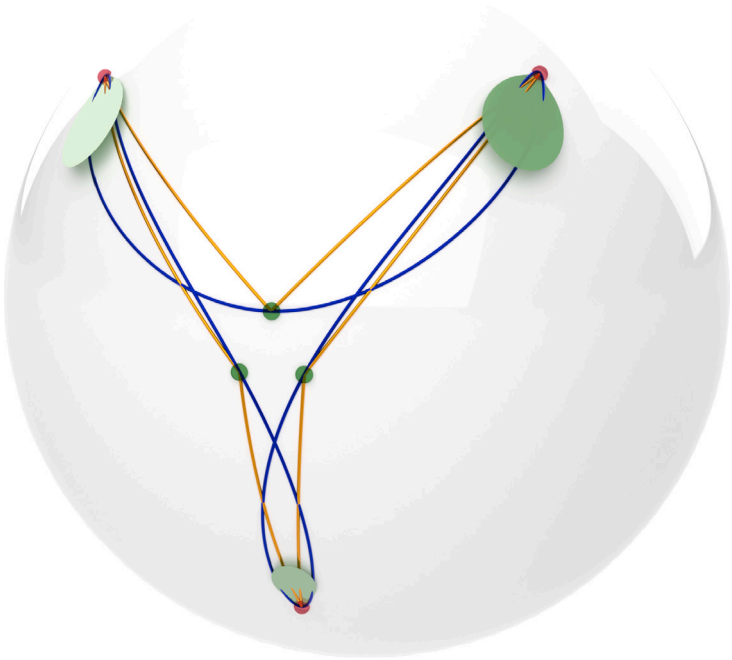

(a)

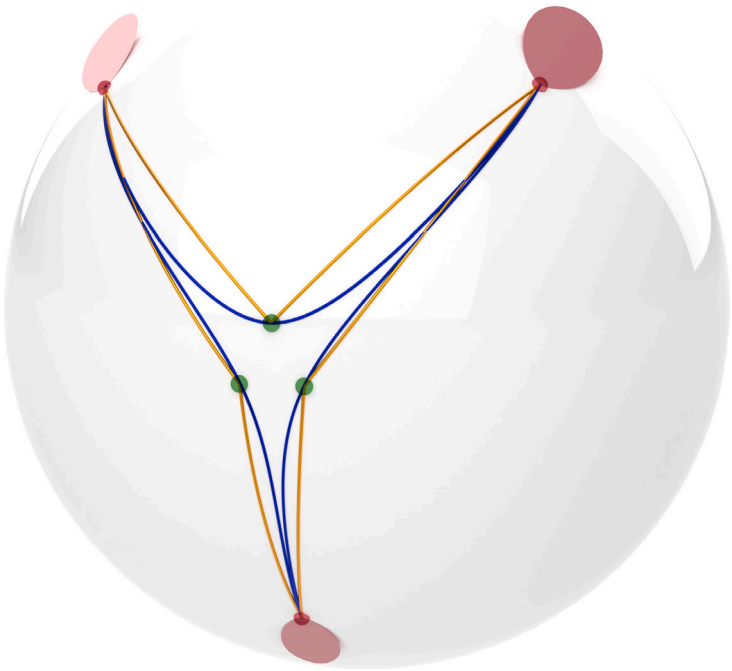

(b)

Fig. 1. On surface renders of the example in Table 1. Interpolation points are represented as glass spheres coloured green/red according as the generalised convexity indicators are positive/negative, respectively. Geodesic arcs between pairs of consecutive interpolation points are depicted as bronze curves. The blue curves are the on-sphere interpolating splines (11) while their geodesic curvature is represented through the ruled surface, formed by the interpolant and its tangential curvature vector distribution (see Struik, 1961, Chapter 4), coloured green/red according to the sign of the geodesic curvature. (For interpretation of the colours in the figure(s), the reader is referred to the web version of this article.)

Table 1
Example 1.

supporting surface	sphere
surface parametrization	$\Big(\cos(u)\sin(v),\ \sin(u)\sin(v),\ \cos(v)\Big)$
number of interpolation points $\mathbf{I}_i$	7
preimages $(u_i, v_i)^T$ of $\mathbf{I}_i$	$\begin{bmatrix}3.141\\2.32\end{bmatrix}, \begin{bmatrix}3.216\\1.635\end{bmatrix}, \begin{bmatrix}3.891\\0.921\end{bmatrix}, \begin{bmatrix}3.141\\1.495\end{bmatrix}, \begin{bmatrix}2.391\\0.921\end{bmatrix}, \begin{bmatrix}3.066\\1.635\end{bmatrix}, \begin{bmatrix}3.141\\2.32\end{bmatrix}$
generalised convexity indicators c_i	$-1,\ +1,\ -1,\ +1,\ -1,\ +1,\ -1$
spline's knot sequence	uniform: $\{t_i,\ i = 0...6\} = \{0,\ 1,\ 2,\ 3,\ 4,\ 5,\ 6\}$
boundary conditions	periodic
initial degrees $\mathcal{K}$ for the spline in Fig. 1a	$\{3,\ 3,\ 3,\ 3,\ 3,\ 3\}$
final $\mathcal{K}$ for the shape-preserving spline in Fig. 1b	$\{6,\ 6,\ 6,\ 6,\ 6,\ 6\}$

Fig. 2. On surface render of a neighbourhood of the near antarctic interpolation point $\mathbf{I}_0 = \mathbf{S}(3.141, 2.32)$ of the example depicted in Fig. 1b.

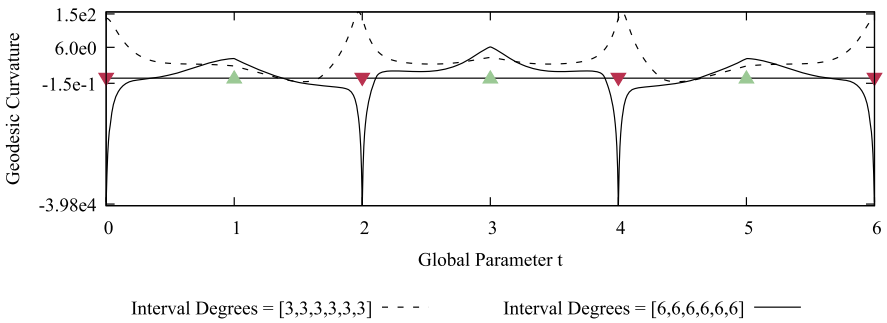

Fig. 3. Logarithmic plot of geodesic curvature of splines depicted in Fig. 1. Specifically, the dashed and solid lines correspond to the splines in Figs. 1a and 1b respectively. The upwards facing green triangles correspond to positive convexity indicators c_i (5) while their red-coloured, downward-facing counterparts to negative c_i.

Theorem 3. $\lim_{k_i \to \infty} \mathbf{c}(t) = \gamma_i(t)$ *uniformly with respect to* $t \in [t_i, t_{i+1}]$, $i \in \{0, 1, ..., n-1\}$.

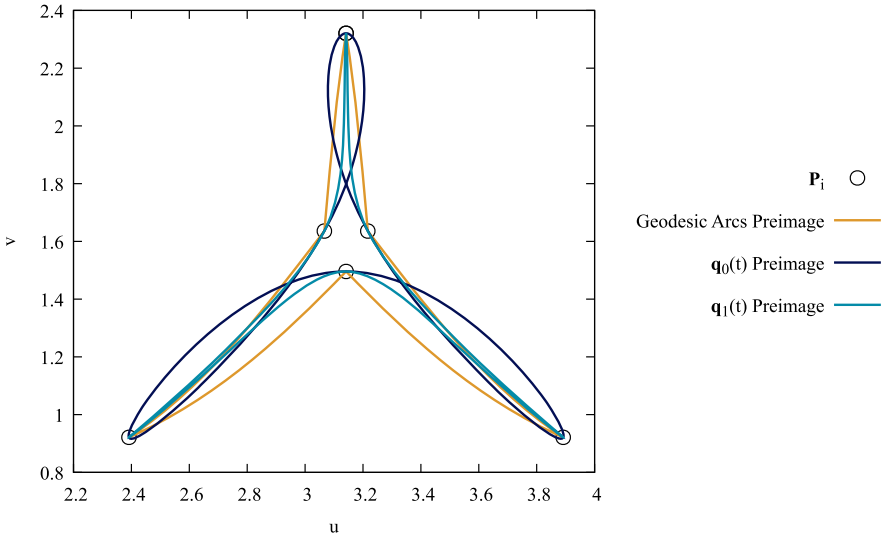

Fig. 4. Preimage of Fig. 1. Specifically, the orange lines are the preimage of the geodesic arcs, while $\mathbf{q}_0$ and $\mathbf{q}_1$ are the preimage of blue splines in Figs. 1a and 1b respectively.

Proof. Substituting $\mathbf{R}_i$, $\mathbf{R}_{i+1}$ (18) into (12),

$$\mathbf{q}(t) = \mathbf{g}_i(t) + \mathbf{R}_i \frac{h_i^2 F_i(1-\tau)}{(d_{i-1}+d_i)} + \mathbf{R}_{i+1} \frac{h_i^2 F_i(\tau)}{(d_i + d_{i+1})} - \ddot{\mathbf{g}}_i(t_i) F_i(1-\tau) - \ddot{\mathbf{g}}_i(t_{i+1}) F_i(\tau). \tag{32}$$

Looking at the definition of $F_i(\tau)$ it is evident that the 4^{th} and 5^{th} terms of (32) are of order $O(k_i^{-2})$ uniformly with respect to t. Now, appealing to (20),

$$\|\mathbf{R}_i h_i^2 F_i(1-\tau)(d_{i-1}+d_i)^{-1}\| \le M |h_i^2 F_i(1-\tau)(d_{i-1}+d_i)^{-1}| = M h_i^2 |(1-\tau)^{k_i} - (1-\tau)| \left(\left(h_{i-1} \frac{k_i}{k_{i-1}} + h_i \right)(k_{i-1}) \right)^{-1}.$$

Noting that for $t \in [t_i, t_{i+1}]$, $|(1-\tau)^{k_i} - (1-\tau)| \le 1$,

$$\|\mathbf{R}_i h_i^2 F_i(1-\tau)(d_{i-1}+d_i)^{-1}\| = O(k_i^{-1})$$

uniformly with respect to t. Proceeding analogously for the third term of (32), we can then write $\mathbf{q}(t) = \mathbf{g}_i(t) + O(k_i^{-1})$. Since $\mathbf{S}(u,v)$ is continuous, it immediately follows that $\mathbf{c}(t) = \mathbf{S} \circ \mathbf{q}(t) = \gamma_i(t) + o(1)$, $t \in [t_i, t_{i+1}]$. □

For the non-local-convexity criterion (i) of Definition 1, however, one can provide different point sets $\mathcal{I}$ on the same, non-developable, surface $\mathbf{S}(u,v)$, for which $\mathbf{c}(t)$ succeeds (see Example 2) or fails (see Example 3) to satisfy the aforementioned criterion.

Example 2. Fig. 5 shows two on-sphere members of the curve family (11), which interpolate the periodic data specified in Table 2. Fig. 6 is a graph of the splines' geodesic curvature, while Fig. 7 depicts their preimages. Notice that in Fig. 6, for degrees equal to $[12, 12, 3, 6, 6, 3]$, $\text{sign}(\kappa_g(t; \mathbf{c})) = -1$ for all t so that $\mathbf{c}$ is a shape-preserving interpolant in accordance with Definition 1

Example 3. Fig. 8 shows two on-sphere members of the curve family (11), which interpolate the periodic data specified in Table 3. Fig. 9 is a graph of the splines' geodesic curvature, while Fig. 10 depicts their preimages. Notice in Fig. 9, that even for degrees as high as 100, the spline's geodesic curvature in $[1,2]$ and $[2,3]$ does not share sign with the neighbouring convexity indicators as is required for the satisfaction of the non-local convexity criterion of Definition 1

3.2.2. Global asymptotic behaviour: developable surfaces

We start by recalling the *first (I)* and the *second II fundamental forms* of a smooth parametric surface $\mathbf{S}(u,v)$, defined as:

$$I = E(du)^2 + 2F\,du\,dv + G(dv)^2, \quad E = \mathbf{S}_u \cdot \mathbf{S}_u,\ F = \mathbf{S}_u \cdot \mathbf{S}_v,\ G = \mathbf{S}_v \cdot \mathbf{S}_v,$$

and

$$II = L(du)^2 + 2M\,du\,dv + N(dv)^2, \quad L = \mathbf{S}_{uu} \cdot \mathbf{n},\ M = \mathbf{S}_{uv} \cdot \mathbf{n},\ N = \mathbf{S}_{vv} \cdot \mathbf{n};$$

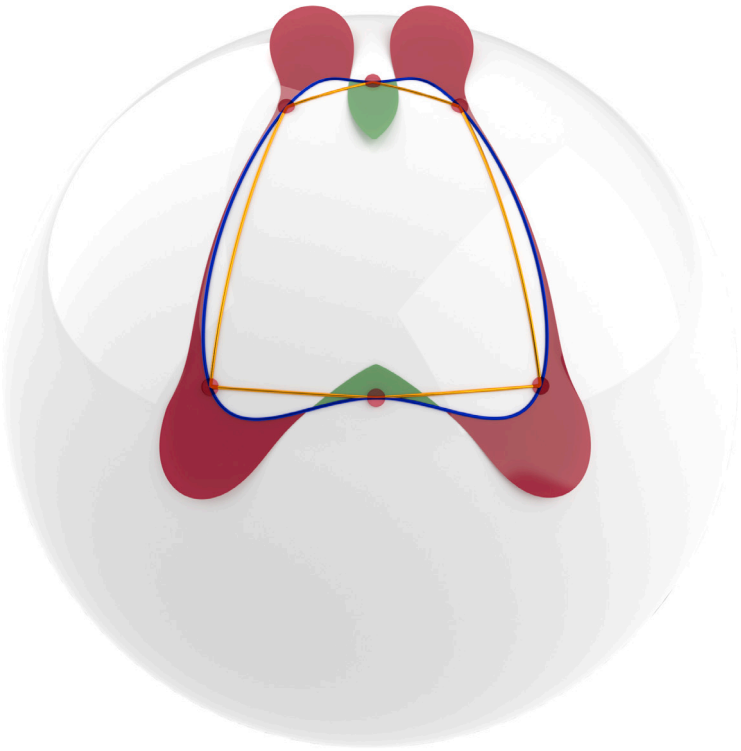

(a)

(b)

Fig. 5. On surface renders of the example in Table 2. For the interpretation of the illustrated items refer to Fig. 1.

Table 2
Example 2.

supporting surface	sphere
surface parametrization	$\left(\cos(u)\sin(v),\ \sin(u)\sin(v),\ \cos(v)\right)$
number of interpolation points $\mathbf{I}_i$	7
preimages $(u_i, v_i)^T$ of $\mathbf{I}_i$	$\begin{bmatrix}1.571\\1.266\end{bmatrix}, \begin{bmatrix}1.964\\1.266\end{bmatrix}, \begin{bmatrix}2.356\\1.266\end{bmatrix}, \begin{bmatrix}2.356\\0.554\end{bmatrix}, \begin{bmatrix}1.964\\0.451\end{bmatrix}, \begin{bmatrix}1.571\\0.554\end{bmatrix}, \begin{bmatrix}1.571\\1.266\end{bmatrix}$
generalised convexity indicators c_i	$-1,\ -1,\ -1,\ -1,\ -1,\ -1,\ -1$
spline's knot sequence	uniform: $\{t_i,\ i = 0...6\} = \{0,\ 1,\ 2,\ 3,\ 4,\ 5,\ 6\}$
boundary conditions	periodic
initial degrees $\mathcal{K}$ for the spline in Fig. 5a	$\{3,\ 3,\ 3,\ 3,\ 3,\ 3\}$
final $\mathcal{K}$ for the shape-preserving spline in Fig. 5b	$\{12,\ 12,\ 3,\ 6,\ 6,\ 3\}$

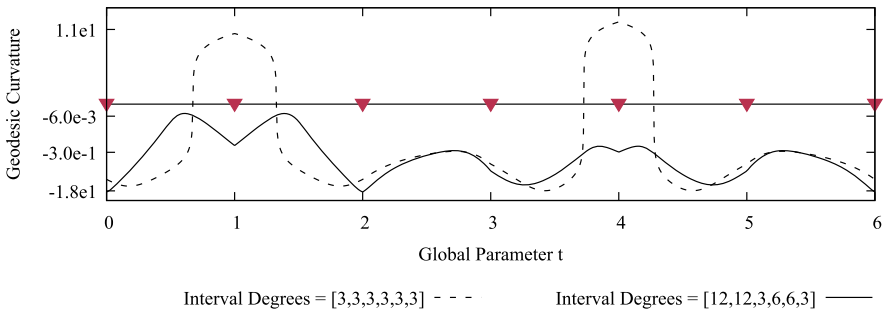

Fig. 6. Logarithmic plot of geodesic curvature of splines depicted in Fig. 5. Specifically, the dashed and solid lines correspond to the splines in Figs. 5a and 5b respectively. The upwards facing green triangles correspond to positive convexity indicators c_i while their red-coloured, downward-facing counterparts to negative c_i.

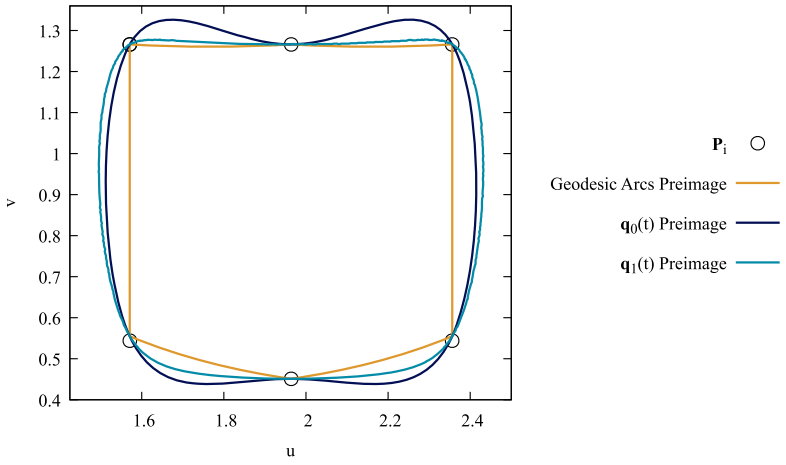

Fig. 7. Preimage of Fig. 5. Specifically, the orange lines are the preimage of the geodesic arcs, while $\mathbf{q}_0$ and $\mathbf{q}_1$ are the preimage of blue splines in Figs. 5a and 5b respectively.

see, e.g., §27 and §38 in Kreyszig (1991). These forms are used to calculate properties of surfaces or entities on them, which remain invariant with respect to parameter transformations, possibly under the additional constraint of constant orientation (i.e., positive Jacobian), such as the curve length, the area, the mean curvature H and the Gaussian curvature K. The latter can be defined as

$$K = \frac{LN - M^2}{EG - F^2};$$

see, e.g., Ch. IV, §14 in Stoker (1989). For *developable surfaces*, the following result holds true (Th. 59.2 in Kreyszig, 1991):

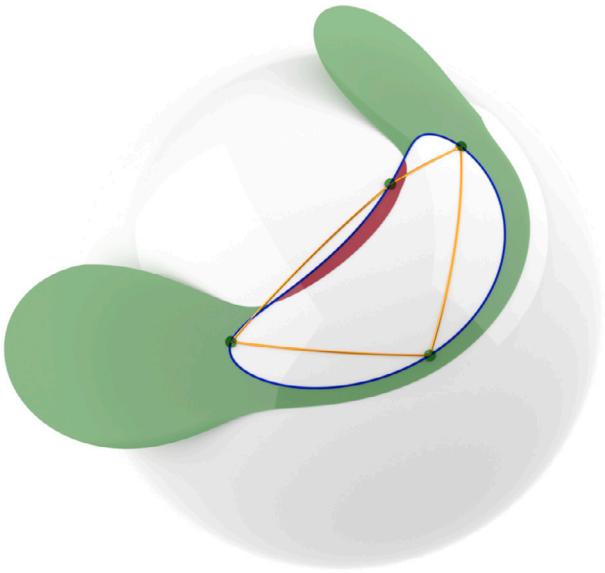

(a)

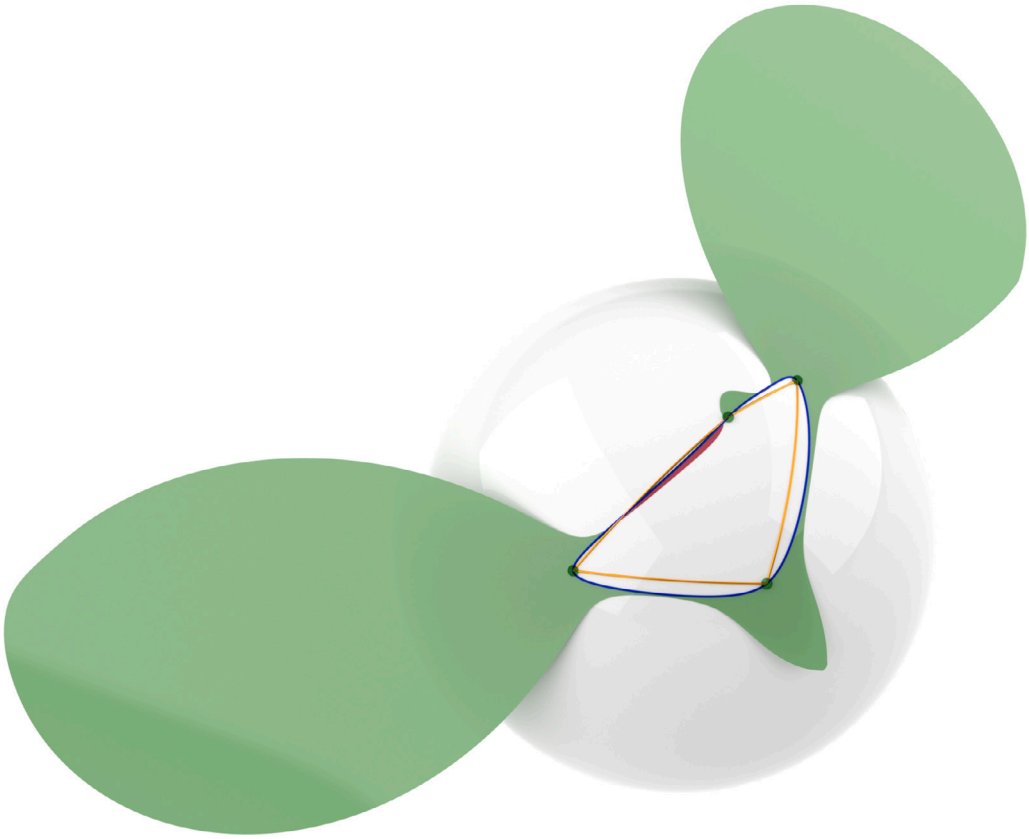

(b)

Fig. 8. On surface renders of the example in Table 3. For the interpretation of the illustrated items refer to Fig. 1.

Table 3
Example 3.

supporting surface	sphere
surface parametrization	$\Big(\cos(u)\sin(v),\ \sin(u)\sin(v),\ \cos(v)\Big)$
number of interpolation points $\mathbf{I}_i$	5
preimages $(u_i, v_i)^T$ of $\mathbf{I}_i$	$\begin{bmatrix}1.571\\1.047\end{bmatrix}, \begin{bmatrix}0.785\\1.047\end{bmatrix}, \begin{bmatrix}1.571\\0.451\end{bmatrix}, \begin{bmatrix}2.356\\0.451\end{bmatrix}, \begin{bmatrix}1.571\\1.047\end{bmatrix}$
generalised convexity indicators c_i	+1, +1, +1, +1, +1
spline's knot sequence	uniform: $\{t_i,\ i = 0...4\} = \{0,\ 1,\ 2,\ 3,\ 4\}$
boundary conditions	periodic
degrees $\mathcal{K}$ for the spline in Fig. 8a	{3, 3, 3, 3}
degrees $\mathcal{K}$ for the spline in Fig. 8b	{9, 9, 9, 9}

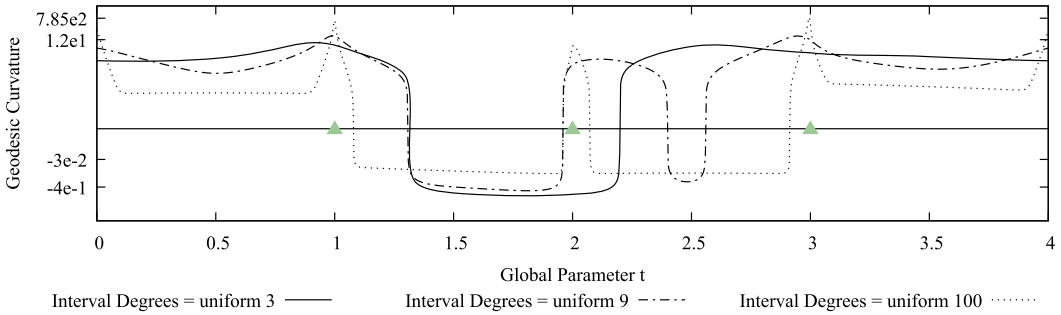

Fig. 9. Logarithmic plot of geodesic curvature of splines depicted in Fig. 8. Specifically, the solid and semi-dashed lines correspond to the splines in Figs. 8a and 8b respectively. The dotted lines correspond to the spline of all degrees equal to 100. The upwards facing green triangles correspond to positive convexity indicators c_i while their red-coloured, downward-facing counterparts to negative c_i.

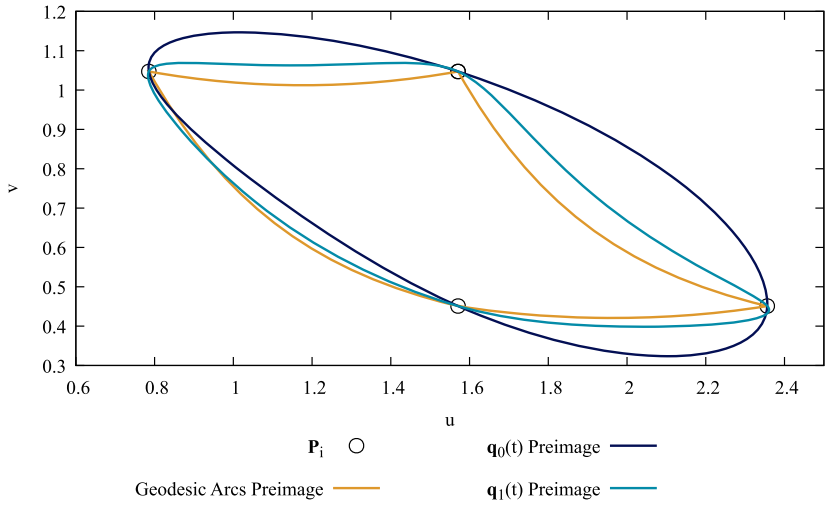

Fig. 10. Preimage of Fig. 8. Specifically, the orange lines are the preimage of the geodesic arcs, while $\mathbf{q}_0$ and $\mathbf{q}_1$ are the preimage of blue splines in Figs. 8a and 8b respectively.

Theorem 4. *A portion* **S** *of a surface which is of class r≥2, i.e., it is parametrizable as a function with continuous (partial) derivatives to the order r, inclusively, is a portion of a developable surface if and only if its Gaussian curvature K is zero everywhere.*

The property which is of interest to us is the fact that developables are the only surfaces, which can be isometrically mapped to the plane (Th. 59.3 in Kreyszig, 1991):

Theorem 5. *A (sufficiently small) portion of a surface of class $r \geq 3$ can be mapped isometrically into a plane if and only if it is a portion of a developable surface*

Therefore, if $\mathbf{S}$ is a developable surface, it can be parametrized by $\mathbf{S}(u,v)$ such that it's first fundamental form is

$$I = (du)^2 + (dv)^2 \tag{33}$$

for a sufficiently small portion of it. We will show that if $\mathbf{c}(t)$ is contained in such a portion and the surface is parametrized in accordance to (33), then for high enough interval degrees it will become a shape-preserving interpolant as in Definition 1. Before proceeding with the asymptotic analysis of $\text{sign}(\kappa_g(t;\mathbf{c}))$, we state two properties of such a parametrization in the form of two lemmata:

Lemma 2. *Let $\mathbf{S}$ be a developable surface parametrized by $\mathbf{S}(u,v)$ as in (33). Then, the second-order partial derivatives $\mathbf{S}_{uu}$, $\mathbf{S}_{uv}$ and $\mathbf{S}_{vv}$ of $\mathbf{S}(u,v)$ are in the direction of the normal vector $\mathbf{n}(u,v)$.*

Proof. First consider the local coordinate system of $\mathbf{S}(u,v)$ defined by $\mathbf{S}_u$, $\mathbf{S}_v$ and $\mathbf{n}$. The relations which express the second derivatives of the surface in terms of this coordinate system are the so-called *formulae of Gauss* (§45 in Kreyszig, 1991) collected in:

Theorem 6. *Let $\mathbf{S}(u,v)$ be a parametric surface of class $r \geq 2$. Then,*

$$\mathbf{S}_{uu} = \Gamma^1_{11}\mathbf{S}_u + \Gamma^2_{11}\mathbf{S}_v + L\mathbf{n}, \quad \mathbf{S}_{uv} = \Gamma^1_{12}\mathbf{S}_u + \Gamma^2_{12}\mathbf{S}_v + M\mathbf{n}, \quad \mathbf{S}_{vv} = \Gamma^1_{22}\mathbf{S}_u + \Gamma^2_{22}\mathbf{S}_v + N\mathbf{n},$$

where Γ^k_{ij} are the Christoffel symbols of the second kind and L, M and N are the coefficients of the second fundamental form of $\mathbf{S}(u,v)$.

Now, Γ^k_{ij} can be expressed in terms on the coefficients of I and their derivatives (§47 in Kreyszig, 1991). Then, due to (33), $E = G = 1$ and $F = 0$ which results in

$$\Gamma^k_{ij} = 0, \quad i,j,k = \{1,2\} \tag{34}$$

In view of (34), Lemma (2) holds by direct application of Theorem 6. □

Lemma 3. *Let $\mathbf{S}$ be a developable surface parametrized by $\mathbf{S}(u,v)$ as in (33). Then the geodesic preimages $\mathbf{g}_i$ (see in (10)) are linear segments.*

Proof. The map $\gamma = \mathbf{S}(\mathbf{g})$ of a preimage curve $\mathbf{g}$ is a geodesic curve on $\mathbf{S}$ if and only if its geodesic curvature vanishes identically (Th. 50.1 in Kreyszig, 1991). Then, if $\mathbf{g}(\mathbf{s}) = (u(s), v(s))^T$ is parametrized with respect to the arc-length s, the following differential equation should hold true (§49 in Kreyszig, 1991):

$$\Gamma^2_{11}\left(\frac{du}{ds}\right)^3 + (2\Gamma^2_{12} - \Gamma^1_{11})\left(\frac{du}{ds}\right)^2 \cdot \frac{dv}{ds} - (2\Gamma^1_{12} - \Gamma^2_{22})\frac{du}{ds} \cdot \left(\frac{dv}{ds}\right)^2 - \Gamma^1_{22}\left(\frac{dv}{ds}\right)^3 + \frac{du}{ds} \cdot \frac{d^2v}{ds^2} - \frac{d^2u}{ds^2} \cdot \frac{dv}{ds} = 0, \tag{35}$$

which, due to (34), degenerates to:

$$\frac{du}{ds} \cdot \frac{d^2v}{ds^2} - \frac{d^2u}{ds^2} \cdot \frac{dv}{ds} = 0 \iff \frac{d\mathbf{g}}{ds} \times_{2D} \frac{d^2\mathbf{g}}{ds^2} = 0,$$

i.e., the curvature of $\mathbf{g}$ vanishes and therefore the preimage $\mathbf{g}$ is a linear segment. □

We can now proceed with the asymptotic analysis of the geodesic curvature of the interpolant $\mathbf{c}(t)$, defined via (11), on a developable surface $\mathbf{S}$, parametrized as in (33) for a portion $\mathbf{S}_0 \subseteq \mathbf{S}$ which contains in $\mathbf{c}(t)$. According to Lemma 2, the second partial derivatives of $\mathbf{S}(u,v)$ will be parallel to the surface normal $\mathbf{n}(u,v)$, which translates to:

$$(\mathbf{S}_i, \mathbf{S}_{jk}, \mathbf{n}) = 0, \quad i,j,k = \{u,v\}.$$

Then the right hand side of (25) vanishes and the numerator of $\kappa_g(t;\mathbf{c})$ (24) can be written as:

$$(\dot{\mathbf{c}}(t), \ddot{\mathbf{c}}(t), \mathbf{n}) = \dot{\mathbf{q}}(t) \times_{2D} \ddot{\mathbf{q}}(t)(\mathbf{S}_u, \mathbf{S}_v, \mathbf{n}), \quad t \in [t_0, t_n].$$

As in (28), due to the orientability assumption for $\mathbf{S}$, a consistent clockwise rotation can be defined on the surface in a continuous manner so that the scalar triple product $(\mathbf{S}_u, \mathbf{S}_v, \mathbf{n})$ retains a constant sign, say positive, throughout the domain of $\mathbf{S}$, so that

$$\text{sign}((\dot{\mathbf{c}}(t), \ddot{\mathbf{c}}(t), \mathbf{n})) = \text{sign}(\dot{\mathbf{q}}(t) \times_{2D} \ddot{\mathbf{q}}(t)), \quad t \in [t_0, t_n]. \tag{36}$$

Therefore the geodesic curvature of $\mathbf{c}$ will share sign with the planar curvature of $\mathbf{q}$. Next, Lemma 3 implies that, if we employ a constant-speed parameterization for $\mathbf{g}_i(t)$, then $\ddot{\mathbf{g}}_i(t) = \mathbf{0}$ and thus:

$$\dot{\mathbf{g}}_i(t) = \text{const} := \dot{\mathbf{g}}_i.$$

Then,

$$\dot{\mathbf{q}}(t) = \dot{\mathbf{g}}_i - h_i\ddot{\mathbf{q}}_i F_i'(1-\tau) + h_i\ddot{\mathbf{q}}_{i+1}F_i'(\tau) \tag{37a}$$

$$\ddot{\mathbf{q}}(t) = \ddot{\mathbf{q}}_i F_i''(1-\tau) + \ddot{\mathbf{q}}_{i+1}F_i''(\tau), \quad \tau = \frac{t-t_i}{h_i}, \quad t \in [t_i, t_{i+1}], \tag{37b}$$

which in its turn gives:

$$\dot{\mathbf{q}}(t) \times_{2D} \ddot{\mathbf{q}}(t) = \dot{\mathbf{g}}_i \times_{2D} \ddot{\mathbf{q}}_i F_i''(1-\tau) + \dot{\mathbf{g}}_i \times_{2D} \ddot{\mathbf{q}}_{i+1}F_i''(\tau) + \ \ddot{\mathbf{q}}_{i+1} \times_{2D} \ddot{\mathbf{q}}_i h_i (F_i''(\tau)F_i'(1-\tau) + F_i'(\tau)F_i''(1-\tau)) \tag{38}$$

Letting $\lambda(t) = \dot{\mathbf{q}}(t) \times_{2D} \ddot{\mathbf{q}}(t)$ and defining

$$\lambda_i := \lambda(t_i) = \dot{\mathbf{g}}_i \times_{2D} \ddot{\mathbf{q}}_i - \ddot{\mathbf{q}}_{i+1} \times_{2D} \ddot{\mathbf{q}}_i h_i (k_i(k_i-1))^{-1}, \tag{39}$$

(38) becomes

$$\lambda(t) = \lambda_i F_i''(1-\tau) + \lambda_{i+1}F_i''(\tau) + \ \ddot{\mathbf{q}}_{i+1} \times_{2D} \ddot{\mathbf{q}}_i h_i \Big[F_i''(\tau)\big(F_i'(1-\tau) + \frac{1}{k_i(k_i-1)}\big) + \big(F_i'(\tau) + \frac{1}{k_i(k_i-1)}\big)F_i''(1-\tau)\Big],$$

which can be written in more compact form as:

$$\lambda(t) = \lambda_i F_i''(1-\tau) + \lambda_{i+1}F_i''(\tau) + \ddot{\mathbf{q}}_{i+1} \times_{2D} \ddot{\mathbf{q}}_i h_i \phi(\tau), \quad \phi(\tau) = \frac{\tau^{k_i-2}(1-\tau)^{k_i-2}}{k_i - 1}$$

Now, consider that the degrees, k_{i-1}, k_i and k_{i+1} in three consecutive intervals, $[t_{i-2}, t_{i-1}]$, $[t_{i-1}, t_i]$ and $[t_i, t_{i+1}]$ increase in accordance to

$$\lim_{k_{j-1}, k_j \to \infty} \frac{k_{j-1}}{k_j} = \kappa_j, \quad j = \{i, i+1\} \tag{40}$$

where κ_j are non-zero positive constants. Recalling Theorem 2 and (36), $\lambda_j \mathrm{c}_j > 0$ for $j = \{i, i+1\}$ for large enough interval degrees. Then, if $\mathrm{c}_i \mathrm{c}_{i+1} > 0$, in order to ensure that $\lambda(t)$ shares sign with c_i, c_{i+1} in $[t_i, t_{i+1}]$ it is sufficient to have:

$$\min_{\tau\in[0,1]} (|\lambda_i F_i''(1-\tau) + \lambda_{i+1}F_i''(\tau)|) > \max_{\tau\in[0,1]} (|\ddot{\mathbf{q}}_{i+1} \times_{2D} \ddot{\mathbf{q}}_i h_i \phi(\tau)|). \tag{41}$$

For the right hand side of (41), the maximum is obtained at $\tau = 0.5$. For the left hand side, the assumption $\lambda_i \lambda_{i+1} > 0$ allows:

$$|\lambda_i F_i''(1-\tau) + \lambda_{i+1}F_i''(\tau)| = |\lambda_i| F_i''(1-\tau) + |\lambda_{i+1}| F_i''(\tau) \geq \min(|\lambda_i|, |\lambda_{i+1}|)(F_i''(1-\tau) + F''(\tau)). \tag{42}$$

Now, the minimum over $\tau \in [0,1]$ of the right hand side of (42) occurs also at $\tau = 0.5$. Therefore, for (41) to be satisfied it is enough that

$$\min(|\lambda_i|, |\lambda_{i+1}|) 2F_i''(0.5) > |\ddot{\mathbf{q}}_{i+1} \times_{2D} \ddot{\mathbf{q}}_i| h_i \phi(0.5) \Leftrightarrow \min(|\lambda_i|, |\lambda_{i+1}|) > |\ddot{\mathbf{q}}_{i+1} \times_{2D} \ddot{\mathbf{q}}_i| h_i 2^{1-k_i}(k_i-1)^{-1},$$

which together with $\lambda_i \lambda_{i+1} > 0$ is a sufficient condition for $\lambda(t)$ to share sign with c_j, $j = \{i, i+1\}$ for all $t \in [t_i, t_{i+1}]$, appealing to (36), we then easily arrive at

Lemma 4. *Let $\mathrm{c}_i \mathrm{c}_{i+1} > 0$ with $\lambda_i \mathrm{c}_i > 0$, $\lambda_{i+1}\mathrm{c}_{i+1} > 0$ and $\min(|\lambda_i|, |\lambda_{i+1}|) > |\ddot{\mathbf{q}}_{i+1} \times_{2D} \ddot{\mathbf{q}}_i| h_i 2^{1-k_i}(k_i-1)^{-1}$. Then the non-local-convexity criterion is satisfied, i.e., the geodesic curvature $\kappa_g(t;\mathbf{c})$ of $\mathbf{c}(t)$ will satisfy $\kappa_g(t;\mathbf{c})\mathrm{c}_j > 0$, $j = \{i, i+1\}$ for all $t \in [t_i, t_{i+1}]$.*

The above lemma provides a sufficient condition for $\mathbf{c}(t)$ to satisfy the *non-local-convexity Criterion* of Definition 1.

To proceed analogously for the *minimum-variation criterion* of Definition 1, we differentiate $\lambda(t)$ with respect to t:

$$\dot{\lambda}(t) = \frac{d}{dt}(\dot{\mathbf{q}}(t) \times_{2D} \ddot{\mathbf{q}}(t)) = \dot{\mathbf{q}}(t) \times_{2D} \mathbf{q}^{(3)}(t). \tag{43}$$

Differentiating (37b), we get:

$$\mathbf{q}^{(3)}(t) = -h_i^{-1}\ddot{\mathbf{q}}_i F_i'''(1-\tau) + h_i^{-1}\ddot{\mathbf{q}}_{i+1}F_i'''(\tau), \quad \text{where } F_i'''(\tau) = (k_i-2)\tau^{k_i-3} \tag{44}$$

Substituting (37a) and (44) in (43) yields:

$$\dot{\lambda}(t) = -\dot{\mathbf{g}}_i \times_{2D} \ddot{\mathbf{q}}_i h_i^{-1} F_i'''(1-\tau) + \dot{\mathbf{g}}_i \times_{2D} \ddot{\mathbf{q}}_{i+1} h_i^{-1} F_i'''(\tau) + \ddot{\mathbf{q}}_{i+1} \times_{2D} \ddot{\mathbf{q}}_i \big(F_i'''(\tau)F_i'(1-\tau) - F_i'(\tau)F_i'''(1-\tau)\big)$$

Recalling (39), the above relation can be written as:

$$\dot{\lambda}(t) = -\lambda_i h_i^{-1} F_i'''(1-\tau) + \lambda_{i+1} h_i^{-1} F_i'''(\tau) + \ \ddot{\mathbf{q}}_{i+1} \times_{2D} \ddot{\mathbf{q}}_i \Big[F_i'''(\tau)\big(F_i'(1-\tau) + \frac{1}{k_i(k_1-1)}\big) - \big(F_i'(\tau) + \frac{1}{k_i(k_1-1)}\big) F_i'''(1-\tau)\Big] \tag{45}$$

Expanding the factor of the third term in the right hand side of (45) gives:

$$F_i'''(\tau)\big(F_i'(1-\tau) + \frac{1}{k_i(k_1-1)}\big) - \big(F_i'(\tau) + \frac{1}{k_i(k_1-1)}\big) F_i'''(1-\tau) = \frac{k_i-2}{k_i-1}\tau^{k_i-3}(1-\tau)^{k_i-3}(1-2\tau),$$

which can be written in more compact form as:

$$\dot{\lambda}(t) = -\lambda_i h_i^{-1} F_i'''(1-\tau) + \lambda_{i+1} h_i^{-1} F_i'''(\tau) + \ddot{\mathbf{q}}_{i+1} \times_{2D} \ddot{\mathbf{q}}_i \chi(\tau), \quad \chi(\tau) = \frac{k_i-2}{k_i-1}\tau^{k_i-3}(1-\tau)^{k_i-3}(1-2\tau). \tag{46}$$

Now, suppose that $\mathrm{c}_i\mathrm{c}_{i+1} < 0$ with $\mathrm{c}_i > 0$ (resp. $\mathrm{c}_i < 0$). If $\dot{\lambda}(t) < 0$ (resp. $\dot{\lambda}(t) > 0$) for $t \in [t_i, t_{i+1}]$, $\mathbf{c}(t)$ will fulfil the minimum-variation criterion in $[t_i, t_{i+1}]$. We first recall that, on the basis of Theorem 2, $\lambda_i\mathrm{c}_i > 0$ and $\lambda_{i+1}\mathrm{c}_{i+1} > 0$ for large enough k_{i-1}, k_i, k_{i+1}. Then, since the first two terms in the right hand side of (46) will both be negative (resp. positive), the following sufficient condition for $\dot{\lambda}(t) < 0$ (resp. $\dot{\lambda}(t) > 0$), $t \in [t_i, t_{i+1}]$ holds true:

$$\min_{\tau\in[0,1]} (|-\lambda_i h_i^{-1} F_i'''(1-\tau) + \lambda_{i+1} h_i^{-1} F_i'''(\tau)|) > \max_{\tau\in[0,1]} (|\ddot{\mathbf{q}}_{i+1} \times_{2D} \ddot{\mathbf{q}}_i \chi(\tau)|).$$

Furthermore, by an argument similar to that used in (42), it is enough to have:

$$h_i^{-1} \min(|\lambda_i|, |\lambda_{i+1}|) \min_{\tau\in[0,1]} (|F_i'''(\tau) + F_i'''(1-\tau)|) > |\ddot{\mathbf{q}}_{i+1} \times_{2D} \ddot{\mathbf{q}}_i| \max_{\tau\in[0,1]} (|\chi(\tau)|). \tag{47}$$

The left hand side of (47) attains its minimum $(k_i-2)2^{4-k_i}$ for $\tau = 0.5$. For the right hand side, we investigate the extrema of $|\chi(\tau)|$:

$$\dot{\chi}(\tau) = \frac{k_i-2}{k_i-1}\tau^{k_i-4}(1-\tau)^{k_i-4}\Big((k_i-3)(1-\tau)(1-2\tau) - (k_i-3)\tau(1-2\tau) - 2\tau(1-\tau)\Big)$$

For $k_i = 3$, $\chi(\tau)$ is a linear segment with $|\chi(\tau)| \le |\chi(0)| = |\chi(1)| = \frac{1}{2}$. For $k_i > 4$, the extrema of $\chi(\tau)$ occur at:

$$\tau_1 = \frac{1}{2} + \sqrt{\frac{1}{2(4k_i-10)}}, \quad \tau_2 = \frac{1}{2} - \sqrt{\frac{1}{2(4k_i-10)}}, \quad \tau_3 = 0, \quad \tau_4 = 1$$

For $k_i = 4$ the extrema of $\chi(\tau)$ occur at τ_1 and τ_2 only. Furthermore, can easily see that:

$$|\chi(\tau_1)| = |\chi(\tau_2)| = 2\frac{k_i-2}{k_i-1}\Big(\frac{k_i-3}{4k_i-10}\Big)^{k_i-3}\sqrt{2(4k_i-10)}^{-1}.$$

Then, since for $k_i > 3$, $|\chi(\tau_3)| = |\chi(\tau_4)| = 0 < |\chi(\tau_1)| = |\chi(\tau_2)|$, we can write:

$$\chi_i := \max_{\tau\in[0,1]} (|\chi(\tau)|) = \begin{cases} \dfrac{k_i-2}{k_i-1}, & k_i = 3 \\ \dfrac{k_i-2}{k_i-1}\Big(\dfrac{k_i-3}{4k_i-10}\Big)^{k_i-3}\dfrac{2}{\sqrt{2(4k_i-10)}}, & k_i > 3 \end{cases} \tag{48}$$

Substituting (48) into (47), the latter becomes:

$$h_i^{-1} \min(|\lambda_i|, |\lambda_{i+1}|)(k_i-2)2^{4-k_i} > |\ddot{\mathbf{q}}_{i+1} \times_{2D} \ddot{\mathbf{q}}_i|\chi_i \Leftrightarrow \min(|\lambda_i|, |\lambda_{i+1}|) > |\ddot{\mathbf{q}}_{i+1} \times_{2D} \ddot{\mathbf{q}}_i| 2^{k_i-4} h_i (k_i-2)^{-1}\chi_i. \tag{49}$$

Combining now Theorem 2, (36) and (49), we arrive at the following

Lemma 5. *Let $\mathrm{c}_i\mathrm{c}_{i+1} < 0$ with $\lambda_i\mathrm{c}_i > 0$, $\lambda_{i+1}\mathrm{c}_{i+1} > 0$ and $\min(|\lambda_i|, |\lambda_{i+1}|) > |\ddot{\mathbf{q}}_{i+1} \times_{2D} \ddot{\mathbf{q}}_i| 2^{k_i-4} h_i (k_i-2)^{-1}\chi_i$, where χ_i is defined as in (48). Then the minimum-variation criterion is satisfied, i.e., there $\exists\ \xi_i \in (t_i, t_{i+1})$ such that the geodesic curvature $\kappa_g(t;\mathbf{c})$ of $\mathbf{c}(t)$ will satisfy $\kappa_g(t;\mathbf{c})\mathrm{c}_i \ge 0$, $t \in [t_i, \xi_i]$ and $\kappa_g(t;\mathbf{c})\mathrm{c}_{i+1} \ge 0$, $t \in [\xi_i, t_{i+1}]$*

Concluding with the *local-co-geodesity criterion*, we note that, since both $\dot{\mathbf{c}}(t)$ and $\dot{\gamma}_l(t)$, $l = \{i-1, i\}$, are continuous in the neighbourhood of the knot $t = t_i$, we can readily provide the following sufficient condition for its satisfaction.

Lemma 6. *Let $\mathrm{c}_i = 0$ and $\delta > 0$. Then, if $\|\dot{\mathbf{c}}(t_i) \times \dot{\gamma}_l(t_i)\| < \delta$, $l = \{i-1, i\}$, then there exists a neighbourhood $\eta_i \subseteq (t_{i-1}, t_{i+1})$ of t_i, such that $\|\dot{\mathbf{c}}(t) \times \dot{\gamma}_l(t_i)\| < \delta$ for all $t \in \eta_i$.*

4. An algorithm for shape-preserving interpolation on developable surfaces

In this section we first prove that, for a set $\mathcal{K}^* = \{k_0^*, ..., k_{n-1}^*\}$ of adequately large degrees, the assumptions of Lemmata 4, 5 and 6 will be satisfied for all intervals and therefore $\mathbf{c}(t)$ will be a shape preserving interpolant according to Definition 1. We then conclude with an algorithm capable to identify such a set $\mathcal{K}^*$ after a finite number of iterations.

In view of Definition 1, we start by introducing the following index sets: let $\mathcal{I}_0 = \{0, ..., n\}$, $\mathcal{I}_1 = \{m \in \mathcal{I}_0 : \mathrm{c}_m \mathrm{c}_{m+n} > 0, n = 1 \text{ or } -1\}$, and $\mathcal{I}_2 = \{m \in \mathcal{I}_0 : \mathrm{c}_m \mathrm{c}_{m+n} < 0, n = 1 \text{ or } -1\}$. For each $i \in \mathcal{I}_1$ such that $i+1$ is also in $\mathcal{I}_1$, let k_{i-1}, k_i and k_{i+1} increase as in (40). On the basis of Theorem 2, we know that there exist $k_{i-1}^{(0)}$, $k_i^{(0)}$ and $k_{i+1}^{(0)}$ such that for all $k_j > k_j^{(0)}$ with $j = \{i-1, i, i+1\}$, we have $\lambda_i \mathrm{c}_i > 0$ and $\lambda_{i+1} \mathrm{c}_{i+1} > 0$. Since $\mathrm{c}_i \mathrm{c}_{i+1} > 0$, we have $\mathrm{c}_j \neq 0$, $j = \{i, i+1\}$ which, looking at (18) and (29), implies that

$$\lim_{k_{i-1}, k_i, k_{i+1} \to \infty} (d_j + d_{j-1}) \ddot{\mathbf{q}}_j = \dot{\mathbf{g}}_j - \dot{\mathbf{g}}_{j-1} \neq \mathbf{0}, \quad j = \{i, i+1\} \tag{50}$$

From (38) and (39) we can write:

$$\lambda_j = \dot{\mathbf{g}}_j \times_{2D} \ddot{\mathbf{q}}_j - \ddot{\mathbf{q}}_{j+1} \times_{2D} \dot{\mathbf{q}}_j h_j (k_j (k_j - 1))^{-1} = \dot{\mathbf{g}}_j \times_{2D} \ddot{\mathbf{q}}_j + O(k_{j-1}^2, k_j^2, k_{j+1}^2)(k_j (k_j - 1))^{-1} = \dot{\mathbf{g}}_j \times_{2D} \ddot{\mathbf{q}}_j + O(1), \quad j = \{i, i+1\},$$

where the last equality holds in view of (40). Now, multiplying (50) by $\dot{\mathbf{g}}_j$, yields:

$$\lim_{k_{i-1}, k_i, k_{i+1} \to \infty} (d_j + d_{j-1}) \dot{\mathbf{g}}_j \times_{2D} \ddot{\mathbf{q}}_j = \dot{\mathbf{g}}_{j-1} \times_{2D} \dot{\mathbf{g}}_j \neq \mathbf{0} \Rightarrow \dot{\mathbf{g}}_j \times_{2D} \ddot{\mathbf{q}}_j = \Theta(k_j, k_{j-1}), \ j = \{i, i+1\}.$$

Then, we can write:

$$|\lambda_j| = \Theta(k_j, k_{j-1}) + O(1) = \Theta(k_j, k_{j-1}), \quad j = \{i, i+1\}. \tag{51}$$

Now, since $2^{1-k_i} = O(2^{-k_i}) = o(k_i^{-1})$,

$$|\ddot{\mathbf{q}}_{i+1} \times_{2D} \ddot{\mathbf{q}}_i| h_i 2^{1-k_i} (k_i - 1)^{-1} = O(k_{i-1}^2, k_i^2, k_{i+1}^2) O(k_i^{-1}) o(k_i^{-1}) = o(1). \tag{52}$$

Therefore, for large enough k_{i-1}, k_i and k_{i+1}, the asymptotic estimates (51) and (52) secure that the inequality assumption of Lemma 4 will always be satisfied since the left hand side dominates the right hand side asymptotically and thus the non-local-convexity criterion in Definition 1 will hold true.

We now analogously proceed for the minimum-variation criterion, investigating the asymptotic validity of the sufficient condition given in Lemma 5:

$$\min(|\lambda_i|, |\lambda_{i+1}|) > |\ddot{\mathbf{q}}_{i+1} \times_{2D} \ddot{\mathbf{q}}_i| 2^{k_i - 4} h_i (k_i - 2)^{-1} \chi_i. \tag{53}$$

From (48) we have:

$$\chi_i = \frac{k_i - 2}{k_i - 1} \left(\frac{k_i - 3}{4k_i - 10} \right)^{k_i - 3} \frac{2}{\sqrt{2(4k_i - 10)}} = \left(\frac{k_i - 3}{2k_i - 5} \right)^{k_i - 3} O(2^{-k_i} k_i^{-1/2}).$$

Then, since

$$\lim_{k_i \to \infty} \left(\frac{k_i - 3}{2k_i - 5} \right)^{k_i - 3} = \lim_{k_i \to \infty} \exp\left((k_i - 3) \ln\left(\frac{1 - 3/k_i}{2 - 5/k_i} \right) \right) = 0 \Rightarrow \left(\frac{k_i - 3}{2k_i - 5} \right)^{k_i - 3} = o(1),$$

we can write:

$$|\ddot{\mathbf{q}}_{i+1} \times_{2D} \ddot{\mathbf{q}}_i| 2^{k_i - 4} h_i (k_i - 2)^{-1} \chi_i = O(k_{i-1}^2, k_i^2, k_{i+1}^2) o(2^{k_i} k_i^{-1} 2^{-k_i} k_i^{-1/2}) = o(k_i^{1/2}). \tag{54}$$

Then, with an identical argument to the convexity criterion, we can secure that (53) is satisfied for large enough degrees and equivalently that the minimum-variation criterion holds true.

Continuing to the local-co-geodesity criterion and guided by Lemma 6, we need only show that if for some $i = \{1, ..., n-1\}$, $\mathrm{c}_i = 0$ and $\dot{\gamma}_{i-1}(t_i) \cdot \dot{\gamma}_i(t_i) > 0$, then

$$\lim_{k_{i-1}, k_i \to \infty} \|\dot{\mathbf{c}}(t_i) \times \dot{\gamma}_l(t_i)\| = 0, \tag{55}$$

where the degrees increase in accordance to (17) and $l = i-1, i$. Introducing the preimages $\mathbf{q} = (u, v)^T$ and $\mathbf{g}_l = (g_l^u, g_l^v)^T$ of $\mathbf{c}$ and γ_l, we can expand $\|\dot{\mathbf{c}}(t_i) \times \dot{\gamma}_l(t_i)\|$ as,

$$\|\dot{\mathbf{c}}(t_i) \times \dot{\gamma}_l(t_i)\| = \left\| \left(\dot{u}(t_i) \mathbf{S}_u(\mathbf{P}_i) + \dot{v}(t_i) \mathbf{S}_v(\mathbf{P}_i) \right) \times \left(\dot{g}_l^u \mathbf{S}_u(\mathbf{P}_i) + \dot{g}_l^v \mathbf{S}_v(\mathbf{P}_i) \right) \right\| = |\dot{\mathbf{q}}(t_i) \times_{2D} \dot{\mathbf{g}}_l| \ \|\mathbf{S}_u(\mathbf{P}_i) \times \mathbf{S}_v(\mathbf{P}_i)\| \quad l = i-1, i. \tag{56}$$

Now, since $\dot{\mathbf{q}}(t)$ is continuous at $t = t_i$, we can substitute either (15a) or (15b) into (56). Choosing the latter, which is expressed on developable surfaces via (37a) for $\tau = 0$, we write

$$\dot{\mathbf{q}}(t_i) \times_{2D} \dot{\mathbf{g}}_l(t_i) = \dot{\mathbf{g}}_i \times_{2D} \dot{\mathbf{g}}_l - h_i F_i'(1) \ddot{\mathbf{q}}_i \times_{2D} \dot{\mathbf{g}}_l + h_i F_i'(0) \ddot{\mathbf{q}}_{i+1} \times_{2D} \dot{\mathbf{g}}_l \quad l = i-1, i \tag{57}$$

Next, consider that by definition $c_i = 0$ implies $(\dot{\gamma}_{i-1}(t_i), \dot{\gamma}_i(t_i), \mathbf{n}(t_i)) = 0$. The first two vectors in this triple product both lie on the tangent plane of $\mathbf{S}(u,v)$ at $(u,v) = \mathbf{P}_i$ and thus they are linearly independent to the third one. It must then be true that $\|\dot{\gamma}_{i-1}(t_i) \times \dot{\gamma}_i(t_i)\| = 0$, which gives:

$$\left\| \left(\dot{g}^u_{i-1} \mathbf{S}_u(\mathbf{P}_i) + \dot{g}^v_{i-1} \mathbf{S}_u(\mathbf{P}_i) \right) \times \left(\dot{g}^u_i \mathbf{S}_u(\mathbf{P}_i) + \dot{g}^v_i \mathbf{S}_u(\mathbf{P}_i) \right) \right\| = |\dot{\mathbf{g}}_{i-1} \times_{2D} \dot{\mathbf{g}}_i| \ \|\mathbf{S}_u(\mathbf{P}_i) \times \mathbf{S}_v(\mathbf{P}_i)\| = 0. \tag{58}$$

Furthermore, if $\mathbf{S}$ is regular in the neighbourhood of $\mathbf{S}(\mathbf{P}_i)$ then $\mathbf{S}_u$ and $\mathbf{S}_v$ are linearly independent which, based on (58), implies that

$$\dot{\mathbf{g}}_{i-1} \times_{2D} \dot{\mathbf{g}}_i = 0. \tag{59}$$

Substituting (59) into (57) and expanding the second and third terms in the right hand side of the latter, we get

$$\dot{\mathbf{q}}(t_i) \times_{2D} \dot{\mathbf{g}}_l(t_i) = -\frac{h_i}{k_i} \ddot{\mathbf{q}}_i \times_{2D} \dot{\mathbf{g}}_l - \frac{h_i}{k_i(k_i - 1)} \ddot{\mathbf{q}}_{i+1} \times_{2D} \dot{\mathbf{g}}_l. \tag{60}$$

Recalling (18) it is easy to see that $\ddot{\mathbf{q}}_{i+1} = O(k_i, k_{i+1})$ and therefore the second term in the right hand side of (60) vanishes as $k_{i-1}, k_i \to \infty$. For the first term, appealing again to (18), we have:

$$\dot{\mathbf{q}}(t_i) \times_{2D} \dot{\mathbf{g}}_l(t_i) = -\frac{h_i}{k_i} \ddot{\mathbf{q}}_i \times_{2D} \dot{\mathbf{g}}_l + O(k_i^{-1}) = -\frac{h_i}{k_i} (d_{i-1} + d_i)^{-1} \left(\dot{\mathbf{g}}_i - \dot{\mathbf{g}}_{i-1} + o(1) \right) \times_{2D} \dot{\mathbf{g}}_l + O(k_i^{-1}) = o(k_i^{-1}) + O(k_i^{-1}), \tag{61}$$

where the last equality holds due to (59). Finally, substituting (56) and (61) into (55), we get

$$\lim_{k_{i-1}, k_i \to \infty} \|\dot{\mathbf{c}}(t_i) \times \dot{\gamma}_l(t_i)\| = \lim_{k_{i-1}, k_i \to \infty} O(k_i^{-1}) \|\mathbf{S}_u(\mathbf{P}_i) \times \mathbf{S}_v(\mathbf{P}_i)\| = 0, \tag{62}$$

Summarising, (52), (54) and (62) yield:

Theorem 7. *Let be given a data set $\mathcal{I}$ with parametrization $\mathcal{T}$ and boundary conditions $\mathcal{B}$ on a developable surface parametrized so that (33) holds true. Then a set of finite degrees $\mathcal{K}^* = \{k_0^*, ..., k_n^*\}$ exists such that $\mathbf{c}(t)$, defined as in (11), is a C^2 shape-preserving interpolant in the sense of Definition 1.*

Guided by Lemmata 4, 5, 6 and Theorem 7, we propose Algorithm 1 for shape-preserving interpolation on developables.

Algorithm 1 aims to identify a set $\mathcal{K} = \{k_i \geq 3\}$ of interval degrees, such that $\mathbf{c}(\mathcal{K})$ is a shape preserving interpolant, in the sense of Definition 1, with the degrees k_i remaining reasonably low. Steps 1 through 3 identify which intervals are relevant to Definition 1 and initialize $\mathcal{K}^{(0)}$ with the minimum possible values for k_i. Then, input to each iteration is a set of degrees $\mathcal{K}^{(j)}$ which define $\mathbf{c}(\mathcal{K}^{(j)})$. Steps 5 through 7 identify in which intervals $\mathbf{c}(\mathcal{K}^{(j)})$ does not satisfy the relevant sufficient conditions developed in §3.2. If these intervals are non-empty, in Step 9, the degrees are increased in accordance to (17) by the minimum possible amount. Notice that for consecutive intervals belonging to the same geodesic arc, their degrees are kept the same in order to achieve visually pleasing results. If more than two intervals are collinear, Algorithm 1 above should be adjusted to ensure all relevant k_i remain identical.

5. Numerical results

Algorithm 1 has been implemented in C++ [1] using the Eigen linear algebra library and the graphic utilities of the Gnuplot software package. The so far numerical experience is in alignment with Kaklis and Sapidis (1995): if the data set does not contain consecutive points along the same geodesic arc, then the algorithm converges after a few iterations to small enough interval degrees. In the case where there are consecutive points along the same geodesic arc, a careful choice of δ in Definition 1 is fundamental to achieving visual pleasantness while keeping the degrees reasonably small. Finally, no data set was identified such that the spline family (11) fails the minimum-variation criterion for uniform degree 3, hinting at the resilience of the spline family to oscillatory behaviour in each interval $[t_i, t_{i+1}]$ when $c_i c_{i+1} < 0$.

In the rest of the section we shall present and discuss the numerical results obtained when applying Algorithm 1 to two data sets on a cone and two data sets on a cylinder with isometric parametrizations given below:

$$\mathbf{S}_{cone}(u,v) = \frac{1}{2}\sqrt{u^2+v^2}\left(\cos\left(2\arctan\left(\frac{v}{u}\right)\right), \sin\left(2\arctan\left(\frac{v}{u}\right)\right), \sqrt{3}\right) \tag{66a}$$

$$\mathbf{S}_{cylinder}(u,v) = \left(\frac{\cos(u)}{4}, \frac{\sin(u)}{4}, v \right) \tag{66b}$$

respectively. In order to secure that the selected geodesics are the one's of minimum length for Examples 4 through 7, the on-surface data sets have been selected such that the shortest linear segment (geodesic-arc preimage) connecting consecutive pre-images of the data is contained continuously in the surface's domain. Further, in these four data sets, two types of boundary conditions (bcs) have been applied: *periodic* and *type-II'-surf* bcs, where the latter can be thought as the analogue of the so-called *natural (type-II')* bcs.

[1] https://github.com/Stamatis8/spin-on-developables.

Algorithm 1

1: Given that $\mathcal{I}_0 = \{0, ..., n\}$, construct the following three sets

$$\mathcal{I}_1 = \{i \in \mathcal{I}_0 : \mathrm{c}_i \mathrm{c}_{i+m} > 0, m = 1 \text{ or } -1\}$$

$$\mathcal{I}_2 = \{i \in \mathcal{I}_0 : \mathrm{c}_i \mathrm{c}_{i+m} < 0, m = 1 \text{ or } -1\}$$

$$\mathcal{I}_3 = \{i \in \mathcal{I}_0 : \mathrm{c}_i = 0 \text{ and } \dot{\mathbf{g}}_{i-1}(t_i) \cdot \dot{\mathbf{g}}_i(t_i) > 0\}$$

2: Fix δ so that $0 < \delta \ll 1$

3: Set $j = 0$ and initialize $\mathcal{K}^{(j)} = \{k_i^{(j)}, \quad i = \{0, ..., n-1\}\}$ to:

$$k_i^{(0)} = 3, \quad i = \{0, ..., n-1\}$$

4: **loop**

5: Compute $\ddot{\mathbf{q}}_i(\mathcal{K}^{(j)})$ by solving the linear system (16a) with appropriate boundary conditions $\mathcal{B}$

6: Compute the following quantities:

$$\lambda_i(\mathcal{K}^{(j)}) \text{ by equation (39)} \qquad \text{for } i \in \mathcal{I}_1 \cup \mathcal{I}_2$$

$$\mu_{i,i+1} = \ddot{\mathbf{q}}_{i+1}(\mathcal{K}^{(j)}) \times_{2D} \ddot{\mathbf{q}}_i(\mathcal{K}^{(j)}) \qquad \text{for } i, i+1 \in \mathcal{I}_1 \cup \mathcal{I}_2$$

$$\tau_{m,i} = \|\dot{\mathbf{c}}(t_i; \mathcal{K}^{(j)}) \times \dot{\gamma}_m(t_i)\|, m = i-1, i \qquad \text{for } i \in \mathcal{I}_3$$

7: Construct the following four index sets:

$$\mathcal{I}_1'(\mathcal{K}^{(j)}) = \{i \in \mathcal{I}_1 : (i+1) \in \mathcal{I}_1, \mu_{i,i+1}(\mathcal{K}^{(j)})\mathrm{c}_i < 0 \text{ and}$$
$$\mu_{i,i+1}(\mathcal{K}^{(j)}) \geq h_i^{-1} 2^{k_i - 1}(k_i - 1) \min(|\lambda_i(\mathcal{K}^{(j)})|, |\lambda_{i+1}(\mathcal{K}^{(j)})|)\}$$

$$\mathcal{I}_2'(\mathcal{K}^{(j)}) = \{i \in \mathcal{I}_2 : (i+1) \in \mathcal{I}_2, \mu_{i,i+1}(\mathcal{K}^{(j)})\mathrm{c}_i > 0 \text{ and}$$
$$\mu_{i,i+1}(\mathcal{K}^{(j)}) \geq h_i^{-1} 2^{4-k_i}(k_i - 2)\chi_i^{-1} \min(|\lambda_i(\mathcal{K}^{(j)})|, |\lambda_{i+1}(\mathcal{K}^{(j)})|)\}$$

$$\mathcal{I}_3'(\mathcal{K}^{(j)}) = \{i \in \mathcal{I}_3 : \tau_{m,i} > \delta, m = \{i-1, i\}\}$$

$$\mathcal{I}_4(\mathcal{K}^{(j)}) = \{i \in \mathcal{I}_1 \cup \mathcal{I}_2 : \lambda_i(\mathcal{K}^{(j)})\mathrm{c}_i < 0\}$$

where χ_i is computed via (48).

8: **if** $\mathcal{I}_1'(\mathcal{K}^{(j)}) \cup \mathcal{I}_2'(\mathcal{K}^{(j)}) \cup \mathcal{I}_3'(\mathcal{K}^{(j)}) \cup \mathcal{I}_4(\mathcal{K}^{(j)}) = \emptyset$ **then stop**

9: **else**

Set $\mathcal{K}^{(j+1)} = \mathcal{K}^{(j)}$
Set $k_m^{(j+1)} = k_m^{(j)} + 1, \quad m = \{i-1, i, i+1\}, \quad i \in \mathcal{I}_1' \cup \mathcal{I}_2'$
Set $k_m^{(j+1)} = \max(k_{i-1}^{(j)}, k_i^{(j)}) + 1, \quad m = \{i-1, i\}, \quad i \in \mathcal{I}_3'$
Set $k_m^{(j+1)} = k_m^{(j)} + 1, \quad m = \{i-1, i\}, \quad i \in \mathcal{I}_4$

10: **end if**

11: **end loop**

Specifically, periodic bcs are applied to data sets $\mathcal{I} = \{\mathbf{I}_i, \ i = 0, ..., n\}$ where $\mathbf{I}_0 = \mathbf{I}_n$ so that

$$\dot{\mathbf{c}}(t_0) = \dot{\mathbf{c}}(t_n), \qquad \ddot{\mathbf{c}}(t_0) = \ddot{\mathbf{c}}(t_n). \tag{67}$$

It can be readily verified that augmenting system (16a) by $\ddot{\mathbf{q}}_0 = \ddot{\mathbf{q}}_n$ and setting $\ddot{\mathbf{q}}_{n+1} := \ddot{\mathbf{q}}_1$ ensures the validity of (67). Next, in the planar case, natural bcs are expressed as zero second derivatives,

$$\ddot{\mathbf{c}}(t_0) = \ddot{\mathbf{c}}(t_n) = \mathbf{0}$$

The straightforward generalization to on-surface curves is that the projections of $\ddot{\mathbf{c}}(t_0)$ and $\ddot{\mathbf{c}}(t_n)$ on the surface's tangent plane are zero. Equivalently,

$$\mathbf{n}(t_0) \times \ddot{\mathbf{c}}(t_0) = \mathbf{n}(t_n) \times \ddot{\mathbf{c}}(t_n) = \mathbf{0} \tag{68}$$

which is set as the defining condition of *type-II'-surf* bcs, when $\mathbf{c}$ lies on a surface $\mathbf{S}$ with normal vector $\mathbf{n}$. Further, it should be noted that *type-II'-surf* bcs imply vanishing geodesic-curvature in analogy to natural bcs implying vanishing planar curvature. In the case of developable surfaces parametrized in accordance with (33), equation (68) is identically translated to the preimage $\mathbf{q}$ of $\mathbf{c}$. More specifically, substituting (23) into (68) and looking at Lemma 2 it follows immediately that,

$$\mathbf{n} \times \left(\mathbf{S}_u \ddot{u}(t_i) + \mathbf{S}_v \ddot{v}(t_i)\right) = \mathbf{0} \iff \mathbf{S}_u \ddot{u}(t_i) + \mathbf{S}_v \ddot{v}(t_i) = \mathbf{0} \iff \ddot{\mathbf{q}}_i = \mathbf{0}, \quad i = 0, \ n \tag{69}$$

In the following examples on developable surfaces, *type-II'-surf* bcs have been secured by augmenting system (16a) with (69).

Table 4
Example 4.

supporting surface	cone
number of interpolation points $\mathbf{I}_i$	5
preimages $(u_i, v_i)^T$ of $\mathbf{I}_i$	$\begin{bmatrix}0.218\\0.421\end{bmatrix}, \begin{bmatrix}0.388\\0.541\end{bmatrix}, \begin{bmatrix}0.558\\0.511\end{bmatrix}, \begin{bmatrix}0.660\\0.466\end{bmatrix}, \begin{bmatrix}0.711\\0.285\end{bmatrix}$
generalized convexity indicators c_i	N/A, +1, +1, +1, N/A
spline's knot sequence	uniform: $\{t_i,\ i=0...4\} = \{0,\ 0.25,\ 0.5,\ 0.75,\ 1\}$
boundary conditions	*type-II'-surf*
final degrees $\mathcal{K}$	$\mathcal{K}(\delta) = \{3,\ 5,\ 5,\ 3\}$

Each example is presented as a pair of data and figures. The data consists of the following items:

1. Type of the supporting surface: cone or cylinder;
2. Number of interpolation (data) points: n;
3. Preimage of the data set on $\mathbb{R}^2 \ni \mathbf{P}_i = (u_i, v_i)^T = \mathbf{S}^{-1}(\mathbf{I}_i)$, $i = \{0, ..., n\}$;
4. Spline's knot sequence: $\mathcal{T} = \{t_i\}$, $i = 0, ..., n$;
5. Boundary conditions: $\mathcal{B} = \{$*type-II'-surf*, periodic$\}$;
6. Interval degrees: $\mathcal{K}(\delta) = \{k_i\}$, $i = 0, ..., n-1$, provided at the final step of Algorithm 1.

In the figures, both the on-surface curves as well as their preimages in the parametric domain are presented. More specifically, on each figure, depicting the supporting surface, the reader can identify:

1. The data set $\mathcal{I} = \{\mathbf{I}_i\}$, $i = 0, ..., n$, as tinted glass spheres. Green/red/clear tint indicates positive/negative/zero generalized convexity indicators c_i (5), respectively;
2. The spline $\mathbf{c}(t)$, as a thin blue-metallic cylindrical tube;
3. The shortest-path geodesic arcs $\gamma_i(t)$, $i = 0, ..., n-1$, as thin bronze cylindrical tubes;
4. The ruled surface, formed by the interpolant and its tangential curvature vector distribution (see Struik, 1961, Chapter 4), represents the geodesic curvature of $\mathbf{c}(t)$ and is coloured green/red according to the sign of $\kappa_g(t; \mathbf{c})$.

Each preimage figure provides the preimages of the data set $\mathbf{P}_i$, the shortest-path geodesic arcs $\mathbf{g}_i$ and all relevant on-surface splines $\mathbf{q}$.

In what follows, four test cases on developable surfaces are documented in Examples 4 through 7. Specifically, Examples 4 and 5 deal with open data-sets on the conical surface (66a), while Examples 6 and 7 deal with open and periodic data-sets respectively on the cylindrical surface (66b). Further, in Examples 4 and 6, the relevant splines initially fail the non-local convexity criterion, while in Examples 5 and 7 they fail the local-co-geodesity criterion.

Example 4. Fig. 11 shows two on-surface members of the curve family (11), which interpolate the data specified in Table 4. Fig. 12 is a graph of the splines' geodesic curvature, while Fig. 13 depicts their preimages. Notice that in Figs. 11a and 12, the geodesic curvature κ_g changes sign in a neighbourhood of the third interpolation point at $t \in [0.5-\epsilon, 0.5+\epsilon]$, violating the non-local convexity-preserving criterion of Definition 1. Applying Algorithm 1, the interval degrees are locally increased to 5, preserving the convexity of the data-set as is evident in Figs. 11b and 12.

Example 5. Fig. 14 shows three on-surface members of the curve family (11), which interpolate the data specified in Table 5. Fig. 15 is a graph of the splines' geodesic curvature, while Fig. 16 depicts their preimages. This example is meant to demonstrate the effect of the user-defined δ parameter on the degree-set resulting from the application of Algorithm 1. The $3^{rd}(t = 0.25)$, $4^{th}(t = 0.5)$ and $5^{th}(t = 0.75)$ data points lie on the same geodesic arc. In view of Fig. 14a, where the spline of uniform degree 3 is rendered, it is evident that, given the choices made: $\delta_1 = 0.1$ and $\delta_2 = 0.01$, the local-co-geodesity criterion is violated for $\|\dot{\mathbf{c}}(t_2) \times \dot{\gamma}_1(t_2)\| = 0.32 > \delta_1$. Next, setting $\delta_1 = 0.1$ and $\delta_2 = 0.01$ and executing Algorithm 1 results in Figs. 14b and 14c, respectively. Notice that in the former case the degrees need only increase from 3 to 6 in order to achieve $\|\dot{\mathbf{c}}(t_2) \times \dot{\gamma}_1(t_2)\| = 0.082 < \delta_1$, while in the latter case they rise considerably to 19 for securing $\|\dot{\mathbf{c}}(t_2) \times \dot{\gamma}_1(t_2)\| = 0.0096 < \delta_2$.

Example 6. Fig. 17 shows two on-surface members of the curve family (11), which interpolate the data specified in Table 6. Fig. 18 is a graph of the splines' geodesic curvature, while Fig. 19 depicts their preimages. Notice that in Fig. 18 the geodesic curvature changes sign in the 3^{rd} parametric interval ($t \in [0.4, 0.6]$) for uniform degree equal to 3, whereas this is not the case when the neighbouring degrees are increased to 4.

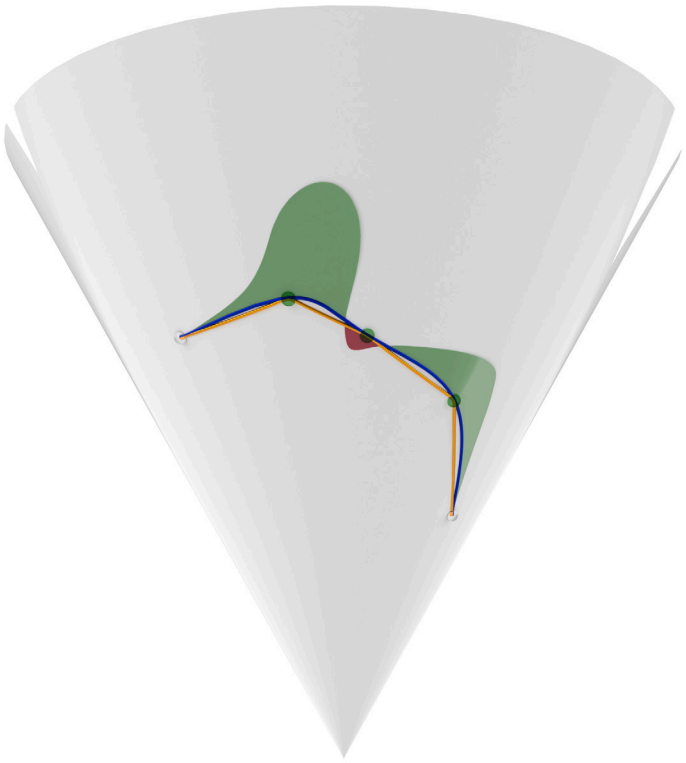

(a)

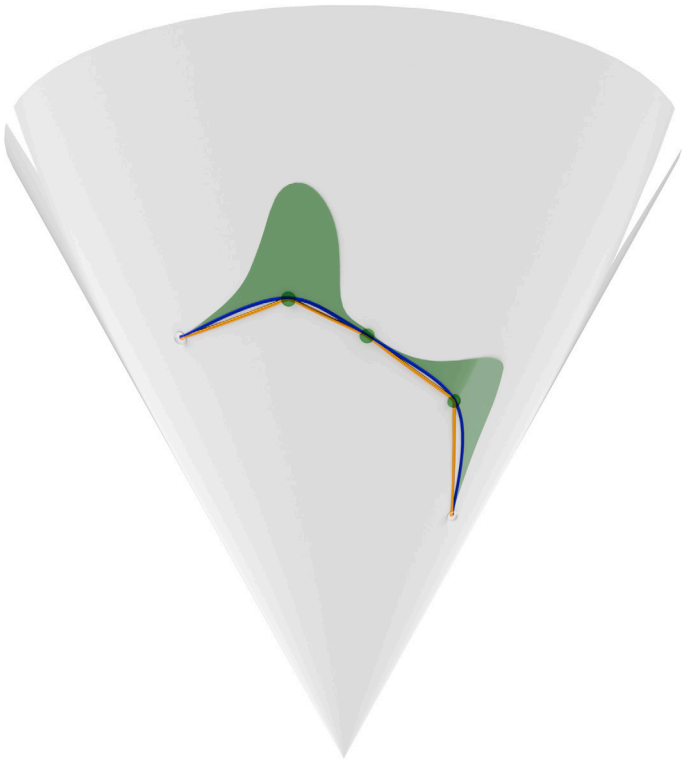

(b)

Fig. 11. On surface renders of the example in Table 4. Fig. 11a corresponds to the respective spline of uniform degree 3 while Fig. 11b to that spline with the degrees listed in Table 4.

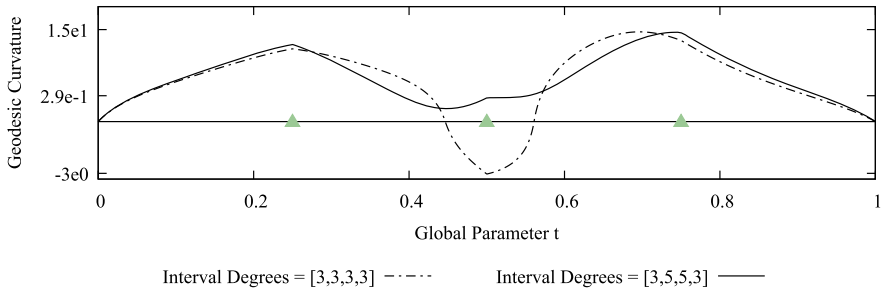

Fig. 12. Logarithmic plot of geodesic curvature of splines depicted in Fig. 11. Specifically, the solid and semi-dashed lines correspond to the splines in Figs. 11b and 11a respectively. The upwards facing green triangles correspond to positive convexity indicators c_i while their red-coloured, downward-facing counterparts to negative c_i.

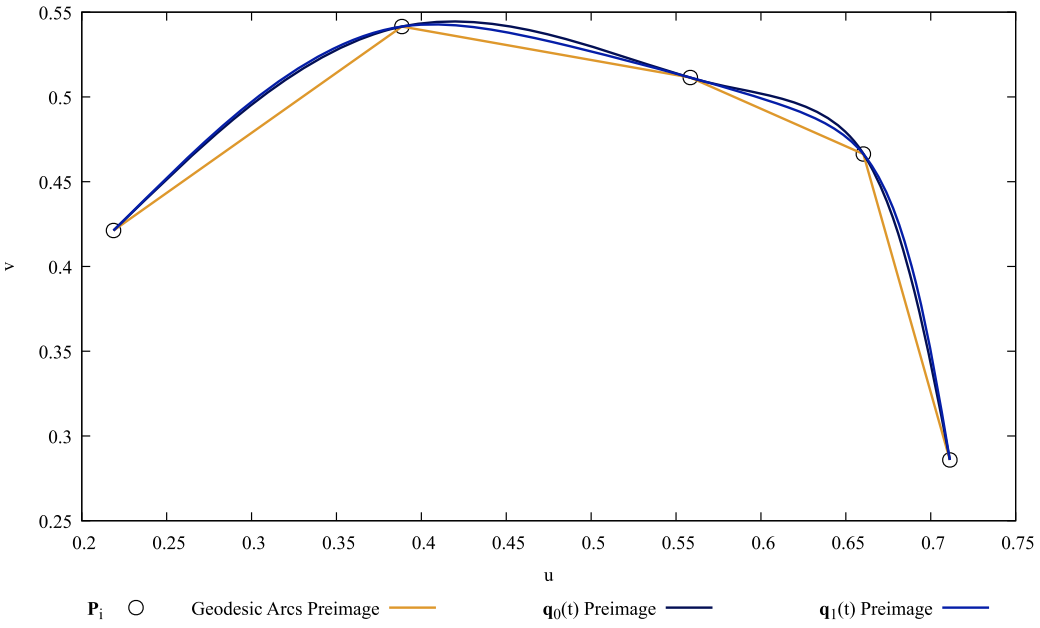

Fig. 13. Preimage of Fig. 11. Specifically, $\mathbf{q}_0(t)$ and $\mathbf{q}_1(t)$ are the preimage of the blue curves in Figs. 11a and 11b respectively.

Table 5
Example 5.

supporting surface	cone
number of interpolation points $\mathbf{I}_i$	5
preimages $(u_i, v_i)^T$ of $\mathbf{I}_i$	$\begin{bmatrix}0.1\\0.9\end{bmatrix}, \begin{bmatrix}0.1\\0.5\end{bmatrix}, \begin{bmatrix}0.3\\0.5\end{bmatrix}, \begin{bmatrix}0.5\\0.5\end{bmatrix}, \begin{bmatrix}0.5\\0.1\end{bmatrix}$
generalized convexity indicators c_i	N/A, -1, 0, $+1$, N/A
spline's knot sequence	uniform: $\{t_i,\ i = 0...4\} = \{0,\ 0.25,\ 0.5,\ 0.75,\ 1\}$
boundary conditions	*type-II'-surf*
final degrees $\mathcal{K}$	$\mathcal{K}(\delta_1 = 0.1) = \{3,\ 6,\ 6,\ 3\}$ $\mathcal{K}(\delta_2 = 0.01) = \{3,\ 19,\ 19,\ 3\}$

Example 7. Fig. 20 shows two on-surface members of the curve family (11), which interpolate the data specified in Table 7. Fig. 21 is a graph of the splines' geodesic curvature, while Fig. 22 depicts their preimages. The 2^{nd} through 4^{th} interpolation points lie on the same geodesic arc, as do the 6^{th} through 8^{th}. Notice that for this data-set, the degrees need to be locally increased to 19 such that the local co-geodesity criterion is satisfied at $\delta = 0.1$, which resulted in degrees of only 6 for Example 5.

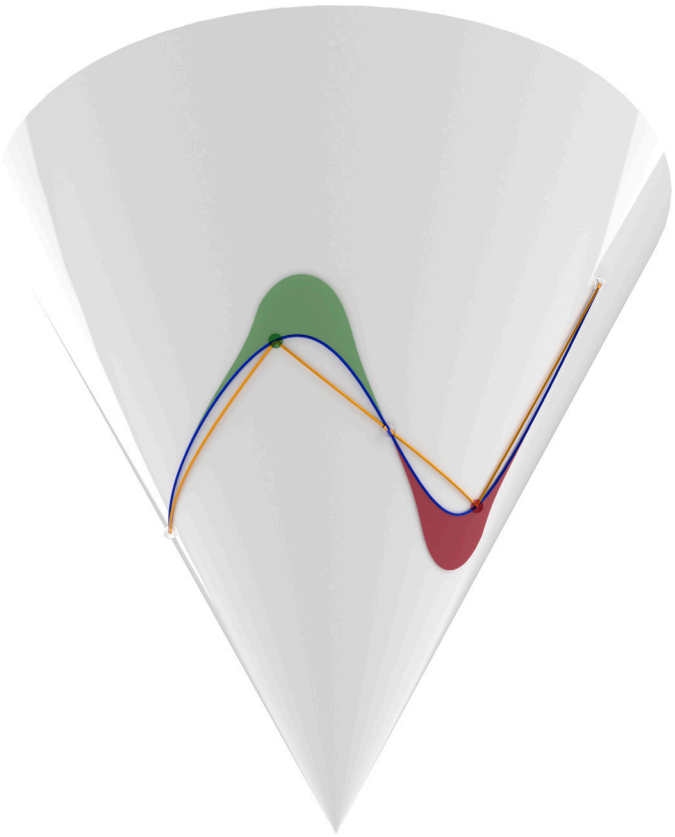

(a)

Fig. 14. On surface renders of the example in Table 5. Fig. 14a corresponds to the respective spline of uniform degree 3 while Figs. 14b and 14c to the splines with degrees $\mathcal{K}(0.1)$, $\mathcal{K}(0.01)$ respectively.

Table 6
Example 6.

supporting surface	cylinder
number of interpolation points $\mathbf{I}_i$	6
preimages $(u_i, v_i)^T$ of $\mathbf{I}_i$	$\begin{bmatrix}1.25\\1.0\end{bmatrix}, \begin{bmatrix}1.75\\0.171\end{bmatrix}, \begin{bmatrix}2.25\\0.05\end{bmatrix}, \begin{bmatrix}2.75\\0.05\end{bmatrix}, \begin{bmatrix}3.25\\0.171\end{bmatrix}, \begin{bmatrix}3.75\\1.0\end{bmatrix}$
generalized convexity indicators c_i	N/A, +1, +1, +1, +1, N/A
spline's knot sequence	uniform: $\{t_i,\ i = 0...5\} = \{0,\ 0.2,\ 0.4,\ 0.6,\ 0.8,\ 1\}$
boundary conditions	*type-II'-surf*
final degrees $\mathcal{K}$	$\mathcal{K}(\delta) = \{3,\ 4,\ 4,\ 4,\ 3\}$

Table 7
Example 7.

supporting surface	cylinder
number of interpolation points $\mathbf{I}_i$	9
preimages $(u_i, v_i)^T$ of $\mathbf{I}_i$	$\begin{bmatrix}0.0\\0.0\end{bmatrix}, \begin{bmatrix}1.176\\0.25\end{bmatrix}, \begin{bmatrix}0.0\\0.5\end{bmatrix}, \begin{bmatrix}-1.176\\0.75\end{bmatrix}, \begin{bmatrix}0.0\\1.0\end{bmatrix}, \begin{bmatrix}1.176\\0.75\end{bmatrix}, \begin{bmatrix}0.0\\0.5\end{bmatrix}, \begin{bmatrix}-1.176\\0.25\end{bmatrix}, \begin{bmatrix}0.0\\0.0\end{bmatrix}$
generalized convexity indicators c_i	−1, −1, 0, +1, +1, +1, 0, −1, −1
spline's knot sequence	uniform: $\{t_i,\ i = 0...8\} = \{0,\ 0.125,\ 0.25,\ 0.375,\ 0.5,\ 0.625,\ 0.75,\ 0.875,\ 1\}$
boundary conditions	periodic
final degrees $\mathcal{K}$	$\mathcal{K}(0.1) = \{3,\ 19,\ 19,\ 3,\ 3,\ 19,\ 19,\ 3\}$

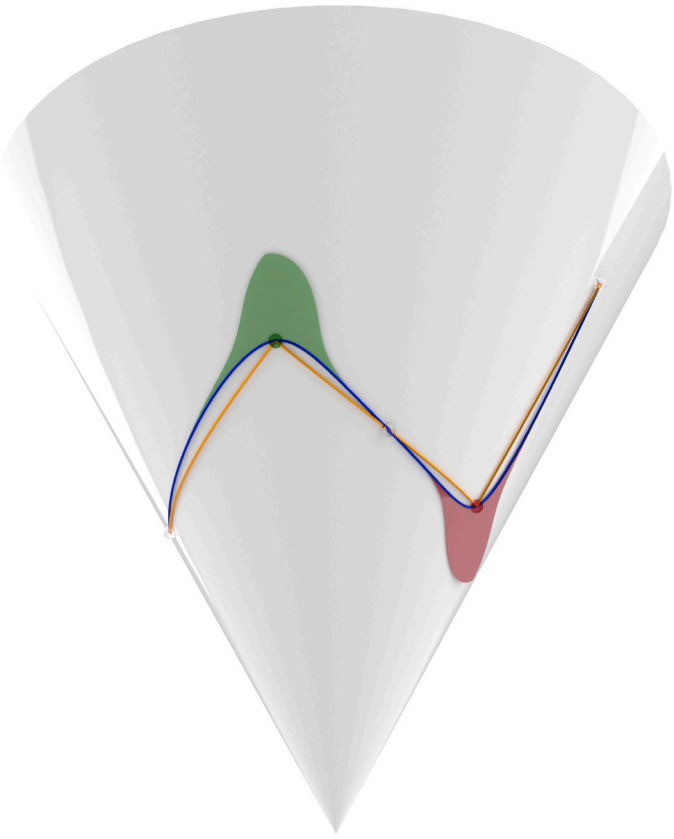

(b)

Fig. 14. (*continued*)

5.1. Geodesic-length parametrization

In this section, the effect of the curve parametrization (12) on the output of Algorithm 1 is investigated via reproducing Examples 4 and 5, parametrized according to the geodesic arc-lengths connecting consecutive data points. Specifically if L_i is the arc-length of $\gamma_i(t)$, define $h_i = L_i / \sum_{i=0}^{n-1} L_i$. Due to the isometric parametrization of the developable surfaces in Examples 4 through 7, this geodesic-based parametrization is equivalent to the standard chord-length parametrization, based on the data point preimages $\mathbf{S}^{-1}(\mathbf{I}_i)$.

In the special case where $\mathbf{S}(u,v)$ is a plane, and thus geodesic arcs degenerate to linear segments, the output of the analogous algorithm was improved Kaklis and Sapidis (1995), identifying degree sequences with smaller degrees compared to the uniform case. Reproducing Examples 4 and 5, parametrized according to geodesic-arc length, it is evident that this trend persists in the current context. Specifically, $\mathcal{K}$ reduces from $\{3,5,5,3\}$ to $\{3,4,4,3\}$ in Example 4 (see Fig. 23) and from $\mathcal{K}(\delta_1 = 0.1) = \{3,6,6,3\}$, $\mathcal{K}(\delta_2 = 0.01) = \{3,19,19,3\}$ to $\{3,5,5,3\}$, $\{3,15,15,3\}$ respectively for Example 5 (see Fig. 24). Notice that due to the smaller degrees necessary for shape preserving interpolation, the geodesic curvature of curves identified through Algorithm 1 is also smaller.

Finally, to further investigate the effect of parametrization on $\mathcal{K}(\delta)$ in Example 5, Algorithm 1 was run for $3 \cdot 10^4$ δ values in $[0.00005, 0.35]$, exploiting the fact that for this example $\mathcal{K}(\delta)$ will be of the form $\{3, f(\delta), f(\delta), 3\}$. Figs. 25 and 26 are plots of $f(\delta)$, for $\delta \in [0.022, 0.35]$ and $\delta \in [0.00005, 0.35]$ respectively. Notice that the degrees generated with the geodesic-based parametrization are always less or equal to the degrees of the uniform case. Further, as δ decreases, they are strictly less, with the difference increasing as is evident from Fig. 26.

6. Conclusions and future work

In this work two criteria for shape-preserving interpolation on smooth surfaces are introduced in §2, both based on the sign of geodesic curvature. The first criterion is of non-local nature (Definition 1), while the second criterion (Definition 2) is a local (weaker) version of the first one. These criteria are tested against a family of on-surface C^2 splines obtained by composing the parametric representation of the supporting surface with the so-called variable-degree (≥ 3) splines amended with the preimages of the shortest-path geodesic arcs connecting each pair of consecutive interpolation points; see in §3.

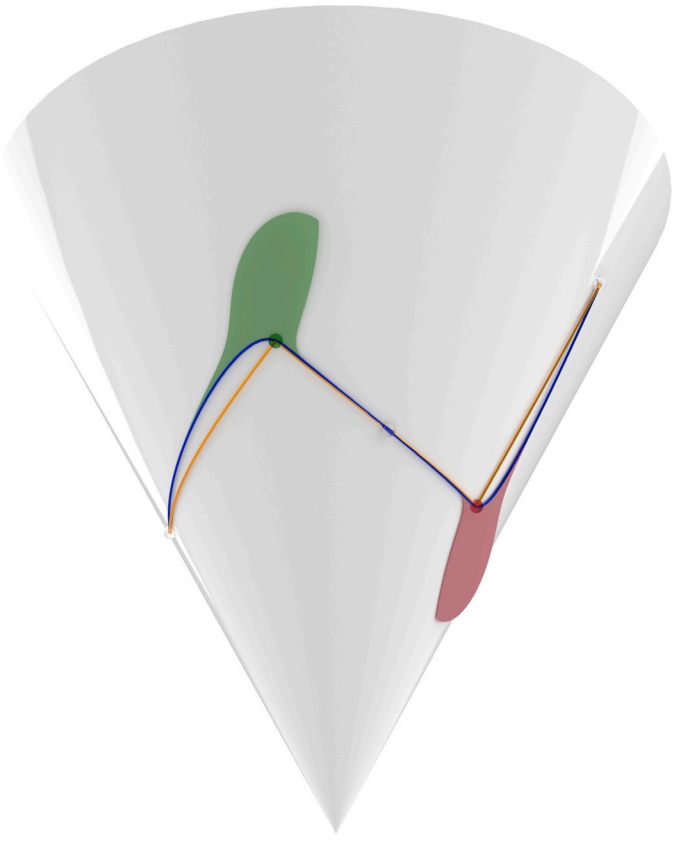

(c)

Fig. 14. (*continued*)

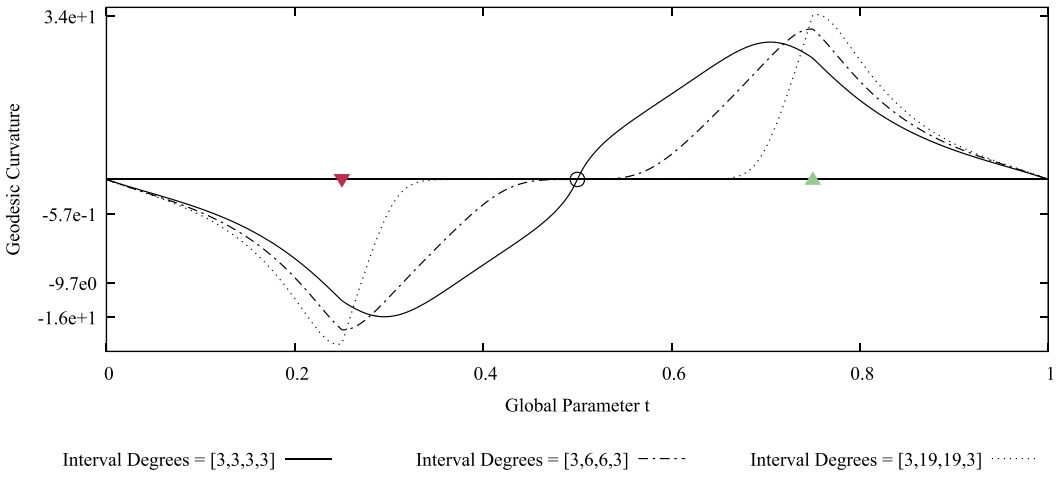

Fig. 15. Logarithmic plot of geodesic curvature of splines depicted in Fig. 14. Specifically, the solid, semi-dashed and dotted lines correspond to the splines in Figs. 14a, 14b and 14c respectively. The upwards facing green triangles correspond to positive convexity indicators c_i while their red-coloured, downward-facing counterparts to negative c_i.

After securing that the interpolation problem is well posed (Theorem 1), we proceed to investigate the asymptotic behaviour of the proposed on-surface splines as degrees increase. Firstly, it is shown that the local-convexity criterion of Definition 2 is satisfied (Theorem 2). Next, moving to non-local asymptotics, we prove that, as degrees increase, the interpolant tends uniformly to the spline curve consisting of the shortest-path geodesic arcs (Theorem 3). Finally, focusing on isometrically parametrized developable surfaces, sufficient conditions are derived (Lemmata 4, 5 and 6), which secure that all criteria of Definition 1 for shape-preserving

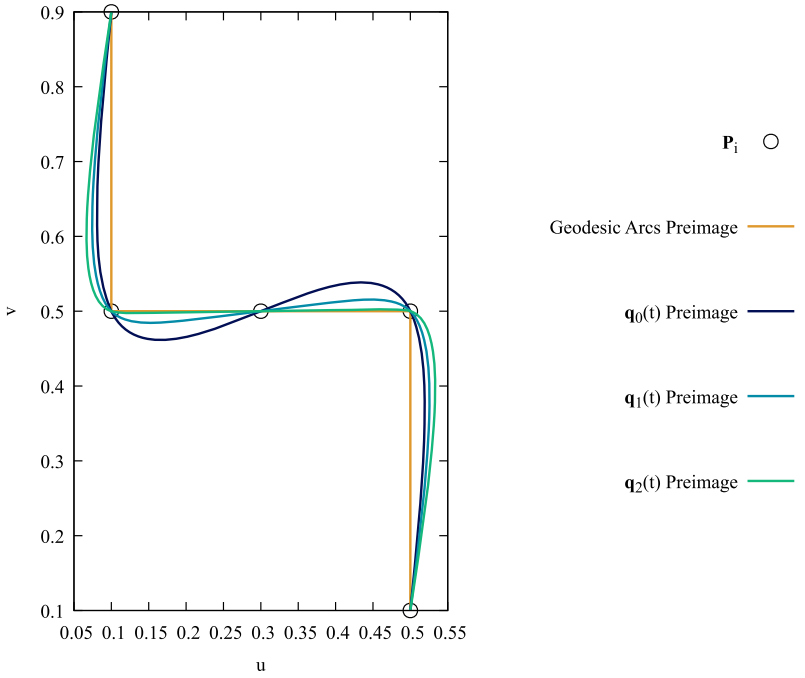

Fig. 16. Preimage of Fig. 14. Specifically, $\mathbf{q}_0(t)$ and $\mathbf{q}_1(t)$ are the preimage of the blue curves in Figs. 14a and 14b respectively.

interpolation on this class of surfaces are satisfied. In §4 it is proved that, for adequately large degrees, the sufficient conditions in the aforementioned lemmata are satisfied (Theorem 7). This yields, in its turn, Algorithm 1 that, after a finite number of iterations, provides a C^2 shape-preserving interpolant for a given data set on a developable surface (§4). Our so far numerical experience indicates that, except from the case of co-geodesic data, the algorithm converges quickly, keeping low the interval degrees (§5).

Future extensions of this work potentially include:

- In analogy with Lemmata 4, 5 and 6, derivation of sufficient conditions for shape-preserving interpolation over classes of non-developable surfaces;
- Amend the spline family introduced in 3 towards improving their capacity to handle the influence of surface properties on the sign of geodesic curvature;
- Embed Algorithm 1 in optimisation setting for computing interval degrees against curve fairness criteria;
- Impact cases that investigate the usefulness of the developed method in industrial applications, e.g., CAD/CAM;
- As rotations in $SO(3)$ can be described via quaternions on the unit sphere $S3$ (see, e.g., Shoemake, 1985), our approach for SP interpolation on $S3$ in the sense of Definition 2, could be useful for SP interpolation in $SO(3)$;
- Embed Algorithm 1 in optimisation setting, e.g., $\texttt{minmax}\{k_i, \forall i : c_i \neq 0\}$ subject to the constraint: `all four index sets in Algorithm 1 are empty`.
- Expand the work for handling shape-preserving approximation on surfaces.

CRediT authorship contribution statement

P.D. Kaklis: Writing – review & editing, Writing – original draft, Supervision, Methodology, Formal analysis, Conceptualization. **S. Stamatelopoulos:** Writing – review & editing, Writing – original draft, Visualization, Validation, Software, Methodology, Formal analysis, Conceptualization. **A.-A.I. Ginnis:** Writing – review & editing, Writing – original draft, Visualization, Software, Methodology, Formal analysis, Conceptualization.

Declaration of competing interest

The authors declare that they have no known competing financial interests or personal relationships that could have appeared to influence the work reported in this paper.

Data availability

Data will be made available on request.

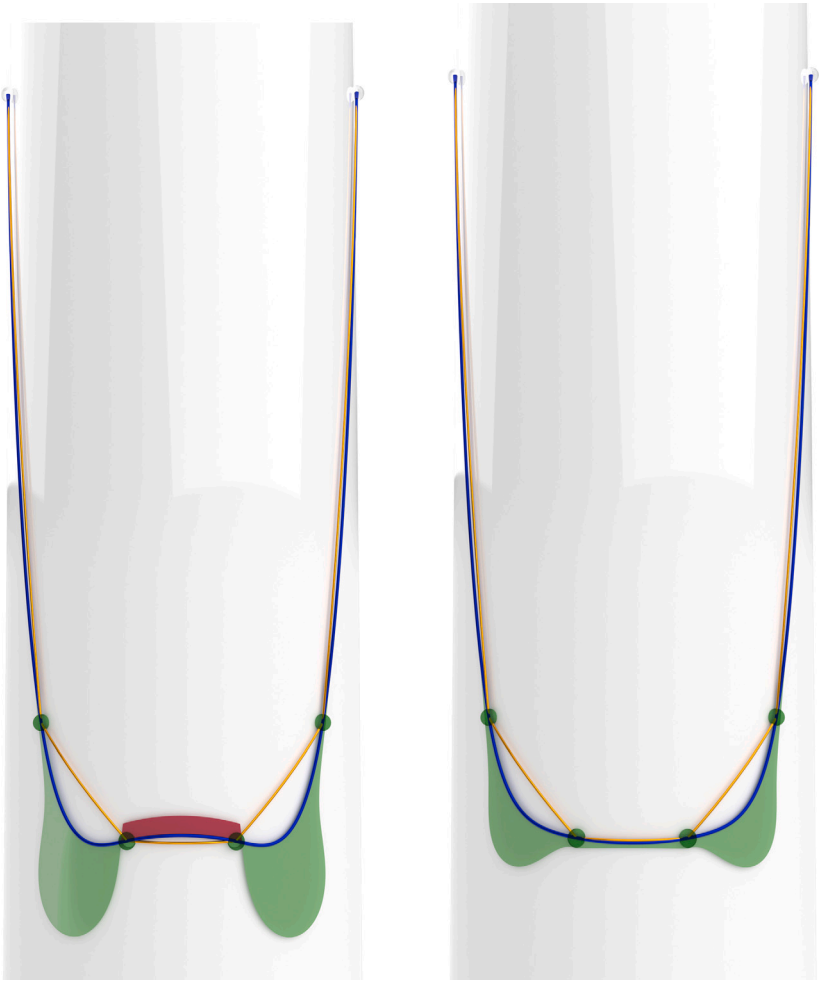

Fig. 17. On surface renders of the example in Table 6. Fig. 17a corresponds to the respective spline of uniform degree 3 while Fig. 17b to that spline with the degrees listed in Table 6.

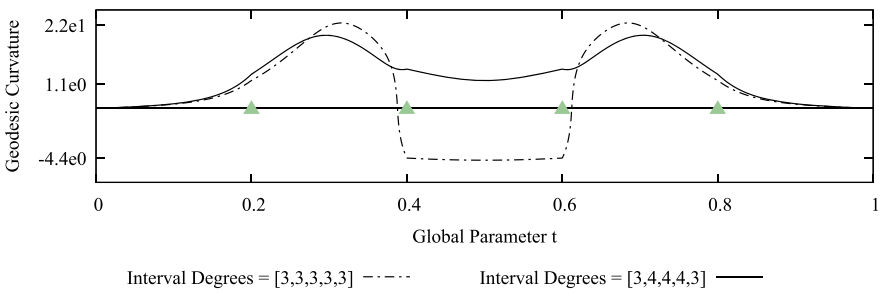

Fig. 18. Logarithmic plot of geodesic curvature of splines depicted in Fig. 17. Specifically, the solid and semi-dashed lines correspond to the splines in Figs. 17b and 17a respectively. The upwards facing green triangles correspond to positive convexity indicators c_i while their red-coloured, downward-facing counterparts to negative c_i.

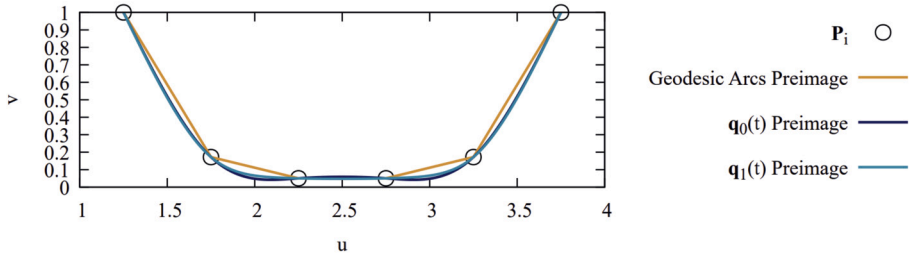

Fig. 19. Preimage of Fig. 17. Specifically, $\mathbf{q}_0(t)$ and $\mathbf{q}_1(t)$ are the preimage of the blue curves in Figs. 17a and 17b respectively.

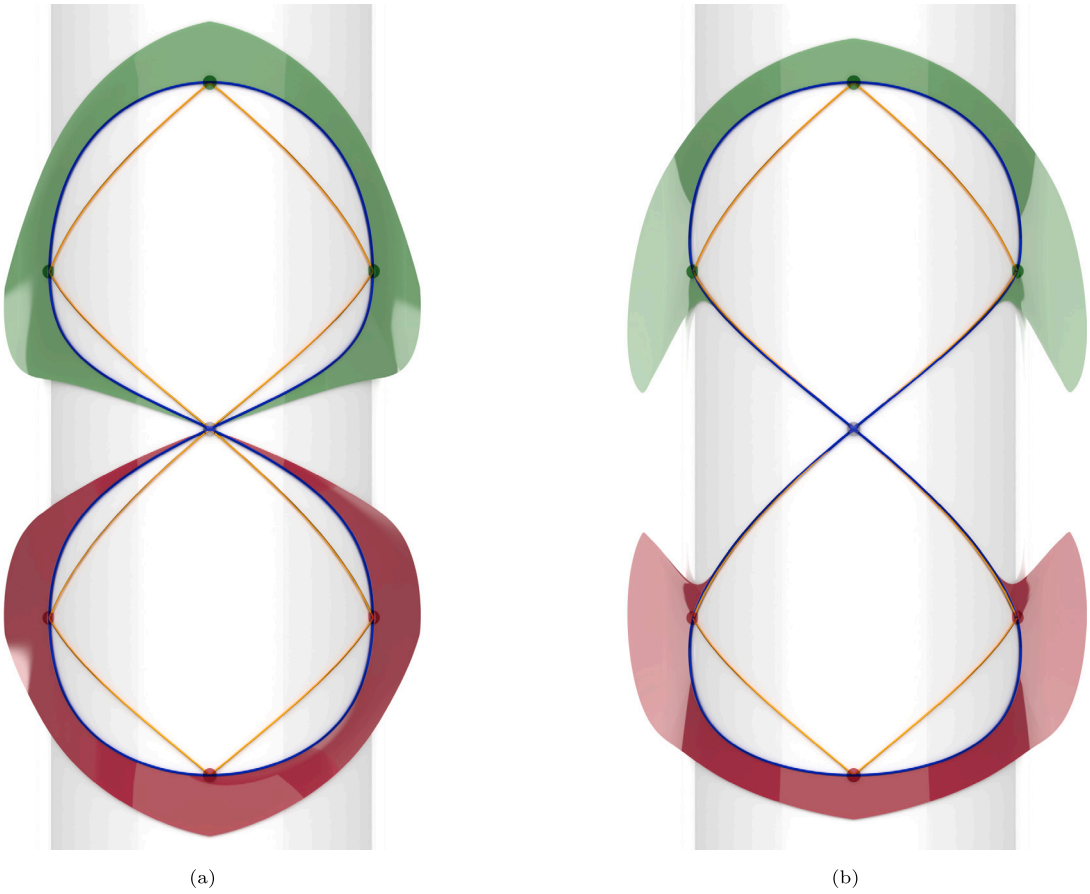

Fig. 20. On surface renders of the example in Table 7. Fig. 20a corresponds to the respective spline of uniform degree 3 while Fig. 20b to that spline with the degrees listed in Table 7.

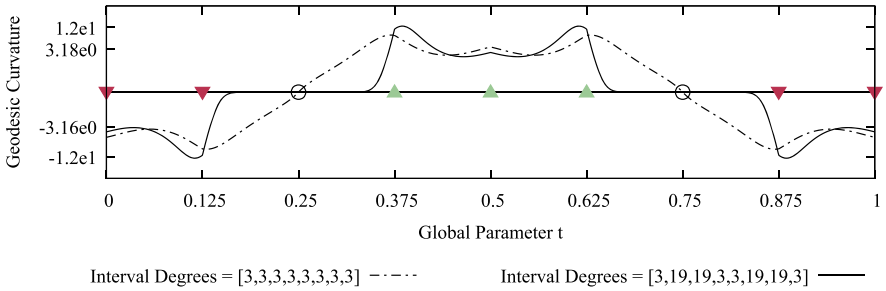

Fig. 21. Logarithmic plot of geodesic curvature of splines depicted in Fig. 20. Specifically, the solid and semi-dashed lines correspond to the splines in Figs. 20b and 20a respectively. The upwards facing green triangles correspond to positive convexity indicators c_i while their red-coloured, downward-facing counterparts to negative c_i.

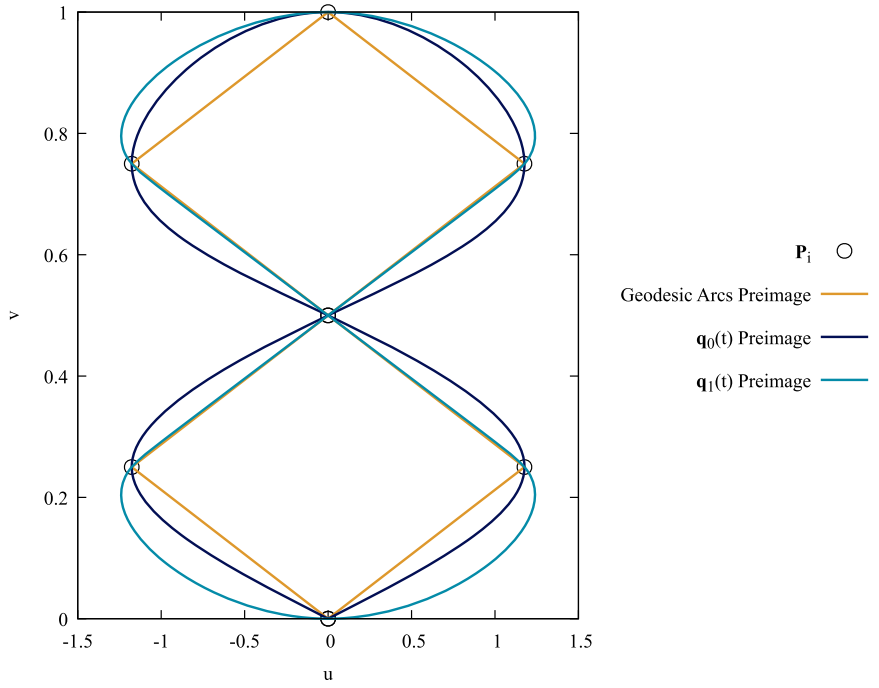

Fig. 22. Preimage of Fig. 20. Specifically, $\mathbf{q}_0(t)$ and $\mathbf{q}_1(t)$ are the preimage of the blue curves in Figs. 20a and 20b respectively.

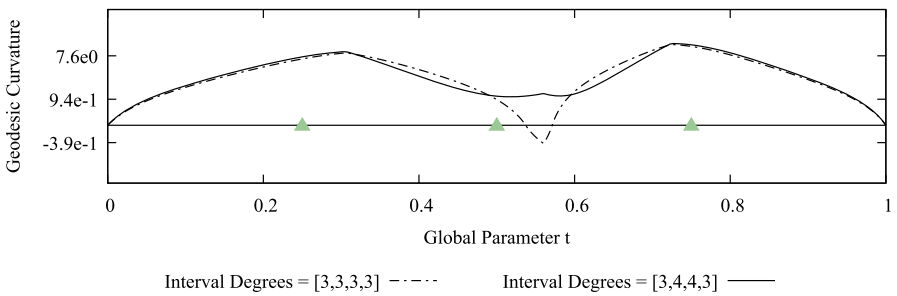

Fig. 23. Reproduction of Fig. 12, this time with the curve $\mathbf{c}(t)$ parametrized relative to geodesic arc-lengths as opposed to uniformly.

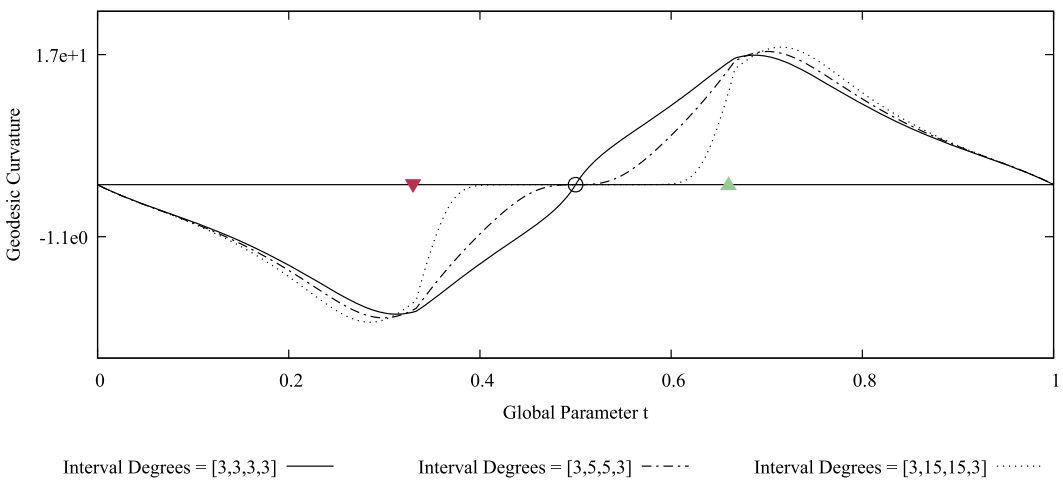

Fig. 24. Reproduction of Fig. 15, this time with the curve $\mathbf{c}(t)$ parametrized relative to geodesic arc-lengths as opposed to uniformly.

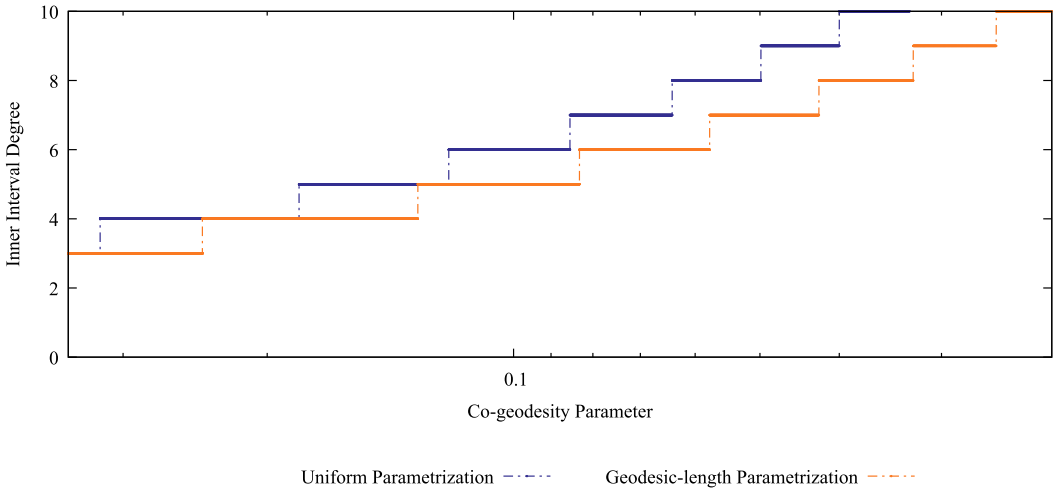

Fig. 25. The resultant degrees $\mathcal{K}(\delta)$ of Example 5 from Algorithm 1 will be of the form $\{3, f(\delta), f(\delta), 3\}$. In this figure, $f(\delta)$ is plotted for $\delta \in [0.022, 0.35]$ for uniform and geodesic-based parametrizations of $\mathbf{c}(t)$.

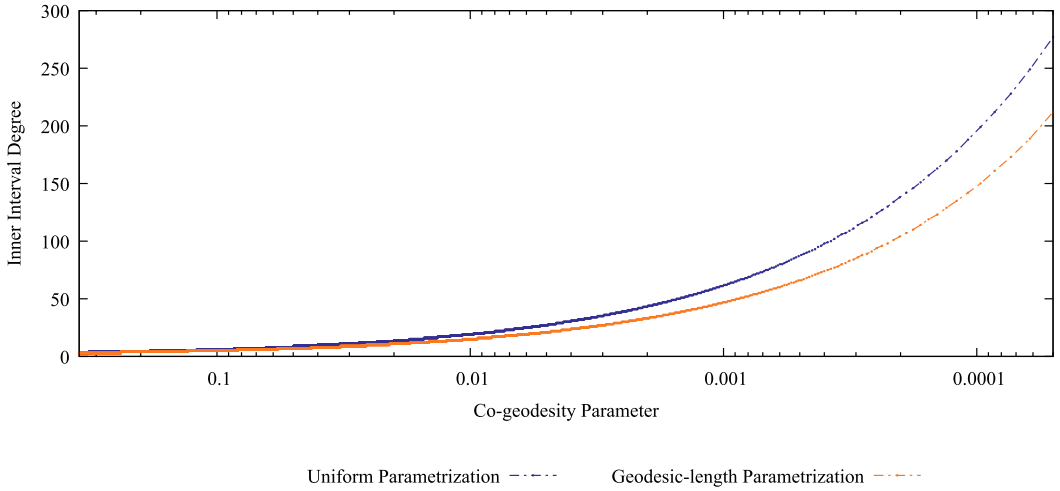

Fig. 26. The resultant degrees $\mathcal{K}(\delta)$ of Example 5 from Algorithm 1 will be of the form $\{3, f(\delta), f(\delta), 3\}$. In this figure, $f(\delta)$ is plotted for $\delta \in [0.00005, 0.35]$ for uniform and geodesic-based parametrizations of $\mathbf{c}(t)$.

Acknowledgements

This work received funding from the European Union's Horizon 2020 Research and Innovation Programme under the Marie Skłodowska-Curie grant agreement No. 860843; project GRAPES (Learning, processing and optimising shapes) http://grapes-network.eu/

References

Arvanitakis, I., Tzes, A., Thanou, M., 2013. Geodesic motion planning on 3D-terrains satisfying the robot's kinodynamic constraints. In: 39th Annual Conference of the IEEE. Industrial Electronics Society, pp. 4144–4149.

Augsdörfer, U.H., Dodgson, N.A., Sabin, M.A., 2010. Variations on the four-point subdivision scheme. Comput. Aided Geom. Des. 27, 78–95.

Azariadis, P.N., Aspragathos, N.A., 2001. Geodesic curvature preservation in surface flattening through constrained global optimization. Comput. Aided Des. 33 (8), 581–591. https://doi.org/10.1016/S0010-4485(00)00102-0.

Bennis, C., Vézien, J-M., Iglésias, G., 1991. Piecewise surface flattening for non-distorted texture mapping. Comput. Graph. 25 (4), 39–46.

Bergmann, R., Gousenbourger, P-Y., 2018. A variational model for data fitting on manifolds by minimizing the acceleration of a Bezier curve. Front. Appl. Math. Stat. 4 (1). https://doi.org/10.3389/fams.2018.00059.

Camarinha, M., Silva Leite, F., Crouch, P.E., 2023. High-order splines on Riemannian manifolds. Proc. Steklov Inst. Math. 321, 172–193.

Costantini, P., 2000. Curve and surface construction using variable degree polynomial splines. Comput. Aided Geom. Des. 5, 419–446.

Costantini, P., Manni, C., 2003. Geometric construction of spline curves with tension properties. Comput. Aided Geom. Des. 20, 579–599.

Costantini, P., Pelosi, F., 2001. Shape-preserving approximation by space curves. Numer. Algorithms 27, 237–264.

Costantini, P., Pelosi, F., 2004. Shape-preserving approximation of spatial data. Adv. Comput. Math. 20, 25–51.

Costantini, P., Goodman, T.N.T., Manni, C., 2001. Constructing C^3 shape preserving interpolating space curves. Adv. Comput. Math. 14, 103–127.
Costantini, P., Kaklis, P.D., Manni, C., 2010. Polynomial cubic splines with tension properties. Comput. Aided Geom. Des. 8, 592–610.
Dierckx, P., 1980. An algorithm for cubic spline fitting with convexity constraints. Computing 24, 349–371.
Dierckx, P., 1996. Curve and Surface Fitting with Splines. Clarendon Press, Oxford.
Dyn, N., Sharon, N., 2017. Manifold-valued subdivision schemes based on geodesic inductive averaging. J. Comput. Appl. Math. 311, 54–67.
Dyn, N., Levin, D., Gregory, J.A., 1987. A 4-point interpolatory subdivision scheme for curve design. Comput. Aided Geom. Des. 4, 257–268.
Dyn, N., Levin, D., Liu, D., 1992. Interpolatory convexity-preserving subdivision schemes for curves and surfaces. Comput. Aided Des. 24, 211–216.
Dyn, N., Hormann, K., Mancinelli, C., 2022. Non-uniform interpolatory subdivision schemes with improved smoothness. Comput. Aided Geom. Des. 94.
Elfving, T., Anderson, L.-E., 1988. An algorithm for computing constrained smoothing spline functions. Numer. Math. 52, 583–595.
Elliott, G.H., 1993. Least squares data fitting using shape preserving piecewise approximations. Numer. Algorithms 5, 365–371.
Ferguson, J.C., Pruess, S., 1991. Shape-preserving interpolation by parametric piecewise cubic polynomials. Comput. Aided Des. 23.
Fletcher, G.Y., McAllister, D.F., 1986. Natural bias approach to shape preserving curves. Comput. Aided Des. 18, 48–52.
Gabriel, S., Kajiya, J., 1985. Spline interpolation in curved space. In: Course Notes for SIGGRAPH '85. ACM Press, New York.
Goodman, T.N.T., Ong, B.H., 1997. Shape preserving interpolation by space curves. Comput. Aided Geom. Des. 15, 1–17.
Goodman, T.N.T., Unsworth, K., 1988. Shape preserving interpolation by curvature continuous parametric curves. Comput. Aided Geom. Des. 5 (4), 323–340.
Gregory, J., 1986. Shape preserving spline interpolation. Comput. Aided Des. 18, 53–57.
Hofer, M., Pottmann, H., 2004. Energy-minimizing splines in manifolds. In: Proceedings of ACM SIGGRAPH 2004. Trans. Graph. 23, 284–293.
Juettler, B., 1997. Shape preserving least-squares approximation by polynomial parametric spline curves. Comput. Aided Geom. Des. 14, 731–747.
Kaklis, P.D., Karavelas, M.I., 1997. Shape-preserving interpolation in R^3. IMA J. Numer. Anal. 17, 373–419.
Kaklis, P.D., Pandelis, D.G., 1990. Convexity-preserving polynomial splines of non-uniform degree. IMA J. Numer. Anal. 10, 223–234.
Kaklis, P.D., Sapidis, N.S., 1995. Convexity-preserving interpolatory parametric splines of non-uniform polynomial degree. Comput. Aided Geom. Des. 12, 1–26.
Karavelas, M.I., Kaklis, P.D., 2000. Spatial shape-preserving interpolation using ν-splines. Numer. Algorithms 23, 217–250.
Kong, V.P., Ong, B.H., 2009. Shape preserving approximation by spatial cubic splines. Comput. Aided Geom. Des. 26 (8), 888–903.
Kreyszig, E., 1991. Differential Geometry. Dover Publications.
Kvasov, B.I., 2000. Methods of Shape-Preserving Spline Approximation. World Scientific Publishing, Ltd.
Lavery, J.E., 2006. Shape-preserving, first-derivative-based parametric and nonparametric cubic L1 spline curves. Comput. Aided Geom. Des. 23 (3), 276–296.
Ma, J-W., Hu, G-Q., Qin, F-Z., Li, G-L., Qu, Z-W., Liu, Y., 2020. Global tool axis vector optimization based on the minimum angular acceleration of rotary axes. Int. J. Adv. Manuf. Technol. 107, 2121–2136.
Morandi, R., Scaramelli, D., Sestini, A., 2000. A geometric approach for knot selection in convexity-preserving spline approximation. In: Laurent, P.J., Sablonnière, P., Schumaker, L.L. (Eds.), Curve and Surface Design. Vanderbilt University Press, Saint-Malo, Nashville, pp. 287–296.
Noakes, L., Heinzinger, G., Paden, B., 1989. Cubic splines on curved spaces. IMA J. Math. Control Inf. 6 (4), 465–473. https://doi.org/10.1093/imamci/6.4.465.
Nyiri, E., Gibaru, O., Auquiert, Ph., 2011. Fast $L_1^k C^k$ polynomial spline interpolation algorithm with shape-preserving properties. Comput. Aided Geom. Des. 28, 65–74.
Patrikalakis, N.M., Bardis, L., 1989. Offsets of curves on rational B-spline surfaces. Eng. Comput. 5, 39–46.
Piazzi, A., Visioli, A., 2000. Global minimum-jerk trajectory planning of robot manipulators. IEEE Trans. Ind. Electron. 47 (1).
Pigounakis, K.G., Kaklis, P.D., 1996. Convexity-preserving fairing. Comput. Aided Des. 28, 981–999.
Pottmann, H., Hofer, M., 2005. A variational approach to spline curves on surfaces. Comput. Aided Geom. Des. 22.
Schmidt, J.W., Scholz, I., 1990. A dual algorithm for convex-concave data smoothing by cubic C^2-splines. Numer. Math. 57, 333–350.
Shoemake, K., 1985. Animating rotation with quaternion curves. In: Proceedings of ACM SIGGRAPH 1985. Trans. Graph. 19 (3), 245–254.
Stoker, J.J., 1989. Differential Geometry. Wiley Interscience.
Struik, D.J., 1961. Lectures on Classical Differential Geometry. Addison-Wesley Series in Mathematics. Addison-Wesley Publishing Company. ISBN 9780486656090.
Wallner, J., 2006. Smoothness analysis of subdivision schemes by proximity. Constr. Approx. 24, 289–318.
Wallner, J., 2020. Geometric subdivision and multiscale transforms. In: Grohs, P., Holler, M., Weinmann, A. (Eds.), Handbook of Variational Methods for Nonlinear Geometric Data. Springer, pp. 121–152.
Wallnerand, J., Dyn, N., 2005. Convergence and C1 analysis of subdivision schemes on manifolds by proximity. Comput. Aided Geom. Des. 22 (7), 593–622.
Wang, Z., Xie, M., 2022. Data approximation by L1 spline fits with free knots. Comput. Aided Geom. Des. 92, 1–12.
Wever, U., 1988. Non-negative exponential splines. Comput. Aided Des. 20 (1), 11–16.
Wu, K-L., Ho, T-J., Huang, S.A., Lin, K-H., Lin, Y-C., Liu, J-S., 2016. Path planning and replanning for mobile robot navigation on 3D terrain: an approach based on geodesic. Math. Probl. Eng. https://doi.org/10.1155/2016/2539761.
Yang, X., 2006. Normal based subdivision scheme for curve design. Comput. Aided Geom. Des. 23 (3), 243–260.